frontiers | Frontiers in Marine Science

TYPE Review
PUBLISHED 20 January 2026
DOI 10.3389/fmars.2025.1747886

OPEN ACCESS

EDITED BY
Khan M. G. Mostofa,
Tianjin University, China

REVIEWED BY
Xiting Liu,
Ocean University of China, China
Debbrota Mallick,
University of Georgia, United States

*CORRESPONDENCE
Hailong Lu
hlu@pku.edu.cn
Hailin Yang
hyang@pku.edu.cn

RECEIVED 17 November 2025
REVISED 30 December 2025
ACCEPTED 30 December 2025
PUBLISHED 20 January 2026

CITATION
Lu Y, Yang H, Xue Y, Tang Y, Xu C and Lu H (2026) Geochemical characteristics of gas hydrate-bearing sediments: insights from a multi-proxy approach.
Front. Mar. Sci. 12:1747886.
doi: 10.3389/fmars.2025.1747886

Geochemical characteristics of gas hydrate-bearing sediments: insights from a multi-proxy approach

Yinghan Lu[1], Hailin Yang[1*], Yuan Xue[1], Yukai Tang[1], Chenlu Xu[2] and Hailong Lu[1,2*]

[1]Beijing International Center for Gas Hydrate, School of Earth and Space Sciences, Peking University, Beijing, China, [2]National Engineering Research Center of Gas Hydrate Exploration and Development, Guangzhou Marine Geological Survey, China Geological Survey, Guangzhou, China

Gas hydrate-bearing sediments are highly sensitive to redox fluctuations, primarily driven by methane fluxes associated with gas hydrate decomposition or cold seep activity. These sediments serve as valuable archives, preserving records of past redox states and methane emission events. Trace elements and rare earth elements (REE) have been widely applied as proxies to reconstruct such environmental conditions. Anoxic, methane-rich depositional environments characteristic of gas hydrate systems promote the enrichment of redox-sensitive major and trace elements (e.g., Fe, Mo, U, Ce) and REE in seep carbonates and surrounding sediments, suggesting that these settings act as important sinks for these elements. Methane also strongly shapes the geochemical signatures, with dynamic seepage events identified through indicators within the sulfate-methane transition zone (SMTZ), such as the barite front, molybdenum enrichment, and authigenic carbonate precipitation. However, relying solely on bulk sediment analysis often leads to ambiguous interpretations. Here we highlight that geochemical signals are fractionated differentially across these phases: carbonates capture fluid signatures, while pyrite hosts sulfur and chalcophile elements (e.g., Mo, As). This review synthesizes and evaluates previous findings, highlighting current knowledge, identifying uncertainties, and outlining directions for future research.

KEYWORDS

gas hydrate-bearing sediments, methane flux, rare earth elements, redox conditions, sedimentary geochemistry, trace elements

1 Introduction

Gas hydrate-bearing sediments are dynamic environments consistently characterized by methane activity, which significantly influences their geochemical characteristics. Understanding the redox conditions within these sediments and the past dynamics of methane seepage is crucial for deciphering past environmental changes and biogeochemical

processes. Inorganic geochemical proxies have emerged as powerful tools for this purpose, offering insights into these complex systems.

Over the past decades, extensive research has been conducted on gas hydrate-bearing environments across various marine regions worldwide, including the South China Sea (Ge et al., 2010; Hu et al., 2015; Li et al., 2016; Sun et al., 2019; Liu et al., 2020), North Sea (Chen et al., 2005), Black Sea (Thiel et al., 2001), Sea of Marmara (Crémière et al., 2013; Yang et al., 2018), Sea of Japan (Snyder et al., 2007; Hiruta et al., 2009), Gulf of Mexico (Feng et al., 2009; Birgel et al., 2011; Hu et al., 2014; Crémière et al., 2016), Gulf of Cadiz (Wang et al., 2015) and some deep-sea fans and deltas (Feng et al., 2010; Rongemaille et al., 2011; Hu et al., 2014; Pierre et al., 2014). These studies have established a valuable foundation for interpreting the geochemical evolution of these unique sedimentary settings.

The behavior of trace elements and rare earth elements (REE) is particularly sensitive to the fluctuating pH and Eh conditions in methane-rich environments. Elements such as Mo, V, U, Ni, Co, Cu, Zn, and Ba are often enriched in cold seep sediments due to their tendency to remain stable under reducing conditions (Francois, 1988; Morford and Emerson, 1999; Russell and Morford, 2001; Tribovillard et al., 2006; Hu et al., 2014; Smrzka et al., 2019, 2020). Their geochemical cycles are intricately linked with authigenic minerals (e.g., carbonates, pyrite, barite) and the redox cycling of Fe and Mn (oxy)hydroxides (Tribovillard et al., 2006; McQuay et al., 2008; Griffith and Paytan, 2012; Large et al., 2017; Smrzka et al., 2020; Yang et al., 2023; Xue et al., 2025). In addition to variations in elemental contents, the distribution patterns and enrichment layers of these element ratios, such as U/Th, V/Cr, Ni/Co (Merinero Palomares et al., 2012; Sun et al., 2019; Algeo and Liu, 2020), and Sr/Ca, Mg/Ca (Bayon et al., 2007; Nöthen and Kasten, 2011), are also considered to be critical factors in the evolution of methane fluxes. Therefore, these trace elements are widely used as proxies for tracing variable redox changes caused by past methane seepage events (Kimura and Watanabe, 2001; Chun et al., 2010; Pälike et al., 2014). Furthermore, REE patterns, including Ce anomalies, are widely applied to reconstruct redox conditions and fluid characteristics (Feng et al., 2009; Ge et al., 2010; Himmler et al., 2010; Rongemaille et al., 2011; Tribovillard et al., 2013).

However, the dynamic nature of cold seep systems, with episodic and transient methane fluxes, leads to highly variable redox conditions. This complexity, coupled with microbial mediation of element migration and transformation (e.g., Fe, Co, Zn, Cu, Ni, B, P, V, W) by sulfate-reducing bacteria or methanogenic/methanotrophic archaea, presents substantial challenges for interpretation (Scherer et al., 1983; Barton et al., 2007; Glass and Orphan, 2012; Glass et al., 2014, 2017). Consequently, relying on a single geochemical proxy is often insufficient to fully unravel the intricate dynamics of gas hydrate-bearing environments.

While inorganic geochemical proxies are widely applied, exclusive reliance on bulk sediment analyses may lead to ambiguous interpretations because bulk sediments integrate terrigenous, biogenic, and authigenic components. Geochemical signals preserved in different sedimentary carriers—namely bulk sediments, authigenic carbonates, and authigenic pyrite—exhibit significant divergence in their formation pathways and sensitivities to methane flux (Tribovillard et al., 2006; Nöthen and Kasten, 2011; Smrzka et al., 2019; Liu et al., 2024). Bulk sediments reflect a mixed signal that is commonly modulated by broader environmental controls, such as sea-level fluctuations and primary productivity (Calvert and Pedersen, 1993; Algeo and Tribovillard, 2009; Chen et al., 2019; Li et al., 2024). In contrast, including carbonates and pyrite, more directly archive pore-fluid composition and seepage intensity (Peckmann et al., 1999, 2001; Chen et al., 2005; Campbell, 2006; Naehr et al., 2007; Smrzka et al., 2019). Cold-seep carbonates, conceptualized as a "Cold-Seep Carbonate Factory" (Dai et al., 2025), precipitate from methane-derived fluids, and their mineralogy (e.g., aragonite versus high-Mg calcite) and elemental ratios (e.g., Sr/Ca and Mg/Ca) are particularly sensitive to variations in fluid flux (Li et al., 2024). Furthermore, authigenic pyrite formed via sulfate-driven AOM (Liu et al., 2024) acts as an important sink for redox-sensitive trace metals (e.g., Mo, As, W) and preserves diagnostic isotopic signatures (e.g., light δ^{98}Mo) associated with benthic Fe–Mn redox shuttling, which may be diluted or obscured in bulk sediment records (Miao et al., 2024b). Therefore, discriminating among these sedimentary carriers is critical for robust reconstruction of past methane seepage.

This review aims to synthesize current knowledge of inorganic geochemical proxies used in gas hydrate-bearing sediments. Specifically, we summarize the indicative value and practical application of proxies such as redox-sensitive trace elements (e.g., Co, Ni, Cu, Zn, V, Mo, U), Fe and Mn speciation, REE patterns (including Ce anomalies), and indicators for reconstructing seepage history (e.g., barite front, Mo enrichment, authigenic carbonate precipitation). Furthermore, we critically analyze and distinguish the specific geochemical signatures recorded in three distinct seepage archives: bulk sediments, authigenic carbonates, and authigenic pyrite. Our goal is to highlight their utility in determining past redox conditions and methane seepage history, and to emphasize the necessity of a multi-proxy approach for a more comprehensive understanding of these dynamic environments.

2 Methane biogeochemistry and geochemical zones in gas hydrate environments

Understanding the roles of redox conditions and biogeochemical processes is essential for sedimentary geochemical research. According to classical early diagenetic theory, organic matter is sequentially degraded using O_2, NO_3^-, Mn(IV), Fe(III) and SO_4^{2-} as different electron acceptors as these become thermodynamically available (Froelich et al., 1979). This process occurs before burial and creates distinct geochemical zones in sediment profiles: the oxygen reduction zone, nitrate reduction zone, manganese reduction zone, iron reduction zone, sulfate reduction zone, and methanogenesis zone. Methane seepage, often derived from hydrate decomposition, usually leads to the

saturation of pore waters with hydrocarbon gases (Johnson et al., 2014). Moreover, the presence of methane enhances biochemical processes in gas hydrate environments. Methane-rich and H_2S-rich fluids modify the distribution of redox zones in marine sediments, thereby creating a more acidic and reducing environment due to the accumulation of CO_2 and H_2S (Niewöhner et al., 1998; Aharon and Fu, 2000; Joye et al., 2010). As a result, the influence of the oxic zone weakens and is replaced by prominent reducing and anaerobic conditions (Chen et al., 2016). Strong methane leakage, such as at cold seeps, can generate large amounts of H_2S, thereby forming a new sulfidic zone (Chen et al., 2016).

In marine sediments, biogeochemical processes such as sulfate reduction (SR), anaerobic oxidation of methane (AOM), and methanogenesis (MOG) collectively shape the geochemical profiles with depth (Goldhaber, 2003; Kong et al., 2021). Sulfate reduction (SR) is the most influential process and occurs mainly in two ways: organoclastic sulfate reduction (OSR) (Berner, 1980) and sulfate-driven anaerobic oxidation of methane (SD-AOM) (Murray et al., 1978; Devol and Ahmed, 1981; Boetius et al., 2000). The two net reactions are expressed stoichiometrically as:

$$2CH_2O + SO_4^{2-} \rightarrow 2HCO_3^- + H_2S$$

$$CH_4 + SO_4^{2-} \rightarrow 2HCO_3^- + HS^- + H_2O$$

Most sulfate is consumed to form sulfide in deeper geochemical profiles. Within these zones, significant amounts of methane are also produced in marine sediments (Jørgensen and Kasten, 2006). Besides SD-AOM, methane can also be oxidized by many alternative electron acceptors, including O_2, NO_3^-, Mn(IV) and Fe(III) oxides, perchlorate (ClO_4^-), and arsenate (As(V)). This occurs due to changes in redox conditions and varying types and rates of organic matter input (Caldwell et al., 2008; Wallenius et al., 2021). Aerobic methane-oxidizing bacteria (MOB), anaerobic methane-oxidizing archaea (ANME), and sulfate-reducing bacteria (SRB) can collectively oxidize methane, coupling AOM with the reduction of oxygen, sulfur, iron, manganese, nitrate, or nitrite (Wallenius et al., 2021) (Figure 1). Some marine methane-seep sediments use manganese oxides (e.g., birnessite) and iron oxides (e.g., ferrihydrite) to oxidize methane (Beal et al., 2009). To date, Fe-AOM and Mn-AOM have been highlighted in many research studies of methane-rich sediments (Sun et al., 2015; Rooze et al., 2016; Li et al., 2019; Liu et al., 2020; Yang et al., 2023; Xue et al., 2025).

As organic matter degrades during sedimentation, it reaches the sulfate-methane transition zone (SMTZ) (Reeburgh, 2007). This zone lies between the sulfate reduction and methanogenesis zones, where downward-diffusing sulfate and upward-diffusing methane meet, react, and are consumed (Barnes and Goldberg, 1976; Borowski et al., 1996, 1999). At this interface, AOM is the key and most active biogeochemical process, which also controls methane release into seawater (Hinrichs and Boetius, 2003; Reeburgh, 2007). AOM primarily occurs in the SMTZ (Knittel and Boetius, 2009) or can also occur in the gas hydrate zone (Cui et al., 2019). AOM is typically coupled to microbial sulfate reduction (MSR) through a reaction involving ANME and SRB (Raghoebarsing et al., 2006; Reeburgh, 2007; Knittel and Boetius, 2009).

The location and morphology of the SMTZ provide valuable information for understanding the occurrence and evolution of gas hydrates. Globally, SMTZ depth is closely related to sedimentation rate, organic matter input, and upward methane flux (Egger et al., 2018). In nearshore and continental shelf sediments, high

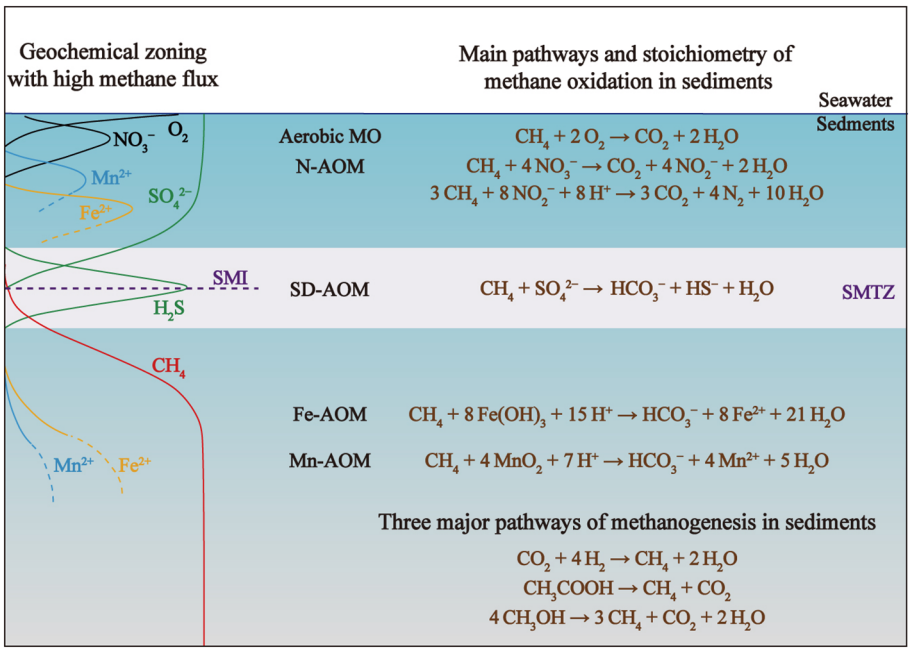

FIGURE 1
Schematic illustration of geochemical zones and methane oxidation (MO) processes in gas hydrate-bearing sediments.

sedimentation and organic matter burial rates lead to a shallow SMTZ, whereas in sediments farther offshore the SMTZ becomes deeper (Egger et al., 2018). Among these factors, upward methane flux is the most important factor affecting the position of the SMTZ and associated biogeochemical processes. Methane flux from gas hydrate decomposition or cold seeps affects sulfate consumption. Strong methane flux from decomposed hydrates or cold seeps accelerates sulfate consumption, thereby changing the SMTZ's depth and thickness within sedimentary sequences (Borowski et al., 1996, 1999; Consolaro et al., 2015). Similarly, seepage intensity strongly affects AOM efficiency: vigorous seepage enhances AOM efficiency, while weak seepage results in less efficient methane oxidation (Joye et al., 2004; Boetius and Wenzhöfer, 2013). Therefore, AOM exerts a primary control on the distribution and thickness of the SMTZ in marine sediments (Borowski et al., 1999). By tracing the typical concentration profiles of methane, sulfate, and their products (sulfide and carbonate), the key characteristics of AOM can be identified (Borowski et al., 1996; Knittel and Boetius, 2009). Based on this understanding, SMTZ characteristics in gas hydrate-bearing sediments can be summarized in two ways (Paull et al., 2005; Castellini et al., 2006):

- In low-flux methane seepage environments, the SMTZ is deeper, thicker, and more stable, and methane may be completely consumed by relatively less efficient AOM.
- In high-flux methane seepage environments, AOM cannot fully balance the upward methane flux, allowing methane to escape directly into the bottom waters. The SMTZ is typically very shallow and varies depending on seepage intensity.

3 Element geochemical proxies of redox environments

3.1 Redox-sensitive trace elements: principles and behavior

Trace elements differ in their sensitivity to redox conditions (Tribovillard et al., 2006), and many show distinctive behavior in methane-rich sediments (Hu et al., 2014; Smrzka et al., 2019, 2020). Among these, Mo, V, U, Ni, and Re are widely regarded as particularly robust proxies for reconstructing paleo-redox conditions, whereas elements such as Co, Cr, Cu, Zn, and Cd may provide complementary information depending on local geochemical and depositional settings (Calvert and Pedersen, 1993; Yarincik et al., 2000; Tribovillard et al., 2006; Algeo and Tribovillard, 2009). Their enrichment generally increases as the environment becomes more reducing, since their solubility is strongly controlled by the redox state, and they accumulate as environmental reducibility increases (Francois, 1988; Morford and Emerson, 1999; Russell and Morford, 2001; Tribovillard et al., 2006). To evaluate their enrichment, enrichment factors (EF) are commonly used (Tribovillard et al., 2006).

The geochemical behavior of these trace elements in methane-rich sediments follows specific patterns (Figure 2). High-valence species of Cr, U, and V are reduced and preferentially enriched under suboxic to anoxic denitrification conditions associated with nitrate reduction, whereas Ni, Cu, Co, Zn, Cd, and Mo are predominantly enriched under euxinic conditions, where free H_2S is produced during sulfate reduction (Algeo and Maynard, 2004; Tribovillard et al., 2006; Smrzka et al., 2020). U, V, and Mo are highly sensitive to hypoxia: concurrent enrichments of these three elements typically indicate euxinic depositional condition, while weaker Mo enrichment may instead reflect an anoxic environment (Algeo and Maynard, 2004; Tribovillard et al., 2006). Ni, Cu, Zn, and Cd are released during organic matter degradation and often fix in sediment via pyrite formation (Huerta-Diaz and Morse, 1990; Morse and Luther, 1999; Tribovillard et al., 2006). Cr is primarily associated with terrigenous components, substituting for Al in clay mineral structures (Björlykke, 1974). Under strongly reducing yet non-sulfidic conditions, V can be immobilized through the formation of vanadium oxides or hydroxide phases, such as VO_2^+ and V(III)-bearing hydroxides [e.g., $V(OH)_3$] (Algeo and Maynard, 2004; Tribovillard et al., 2006). Rhenium (Re) is sensitive to dissolved oxygen and serves as a proxy for oxygen penetration depth at seep sites (Smrzka et al., 2020).

3.1.1 Trace element enrichment

The cycling of redox-sensitive elements is significantly affected by abundant H_2S and CH_4 from seepage (Figure 2; Tribovillard et al., 2013; Hu et al., 2015; Smrzka et al., 2020). Methane derived from gas hydrate decomposition reacts with pore water SO_4^{2-}, producing H_2S via AOM-MSR (Boetius et al., 2000; Knittel and Boetius, 2009). Such reactions commonly lead to anoxic or sulfidic conditions (Chen et al., 2016; Sun et al., 2019).

Case studies from different seep and hydrate systems illustrate the variability of trace element enrichment patterns. For example, Feng et al. (2010) found highly variable V, Mo, U, and Cd contents in seep authigenic carbonates from the northern Congo fan, which increased during periods of relatively high fluxes. Ge et al. (2010) reported that Mo, U, Ni, V, and Co recorded anoxic conditions during carbonate precipitation on the northern continental slope of the South China Sea. Deng et al. (2017) noted that gas hydrate-bearing sediments in the South China Sea were more enriched in Sr, Pb, Th, U, Zn, Cu, and Mo relative to the upper crust. Wang et al. (2019) applied tungsten (W) as a novel proxy in seep carbonate systems, noting its biological role in microbial AOM pathways (Barton et al., 2007; Glass and Orphan, 2012).

In contrast, Chen et al. (2016) observed that although Mo exhibited expected enrichment in sulfidic environments, Co, Cu, Ni, Zn, and V showed little enrichment during active methane seepage. They attributed this to weak OSR under low TOC conditions. Based on these results, Mo and U emerge as the most reliable indicators of methane seepage among redox-sensitive trace elements, with AOM-driven sulfidic conditions enhancing Mo accumulation (Chen et al., 2016). This interpretation is further confirmed by reports of extreme Mo enrichments ($Mo_{EF} > 10$) and seawater-like Mo_{EF}/U_{EF} values in gas hydrate-bearing sediments worldwide (Hu et al., 2014, 2015; Chen et al., 2016; Deng et al., 2017; Liu et al., 2020).

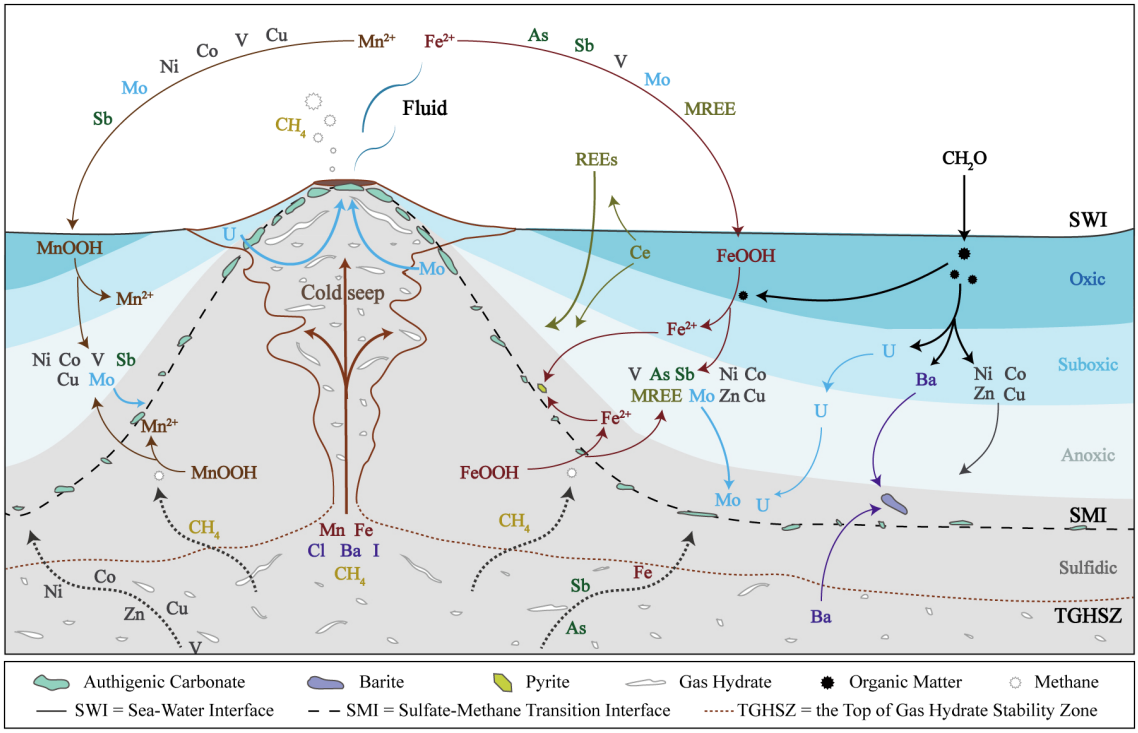

FIGURE 2
Migration processes of trace elements in cold seep environments.

The Mo-U pattern in sediments provides a widely applied proxy for depositional redox states (Figure 3). Mo typically occurs as soluble molybdate (MoO_4^{2-}) under oxic conditions, but under reducing conditions it is reduced and removed from solution, commonly through transformation to lower-valence Mo species (Mo(VI) → Mo(IV)/Mo(V)) and subsequent fixation in sulfide- or organic-associated phases (Calvert and Pedersen, 1993). U is soluble as U (VI) under oxic conditions but is reduced and fixed in sediments as U (IV) under anoxia (Tribovillard et al., 2006). Thus, Mo and U enrichments jointly reflect the redox gradient: U is commonly removed at the Fe^{2+}–Fe^{3+} transition zone (suboxic), whereas Mo requires sulfidic conditions (Morford and Emerson, 1999; Algeo and Tribovillard, 2009; Scott and Lyons, 2012; Tribovillard et al., 2012). Algeo and Tribovillard (2009) and Tribovillard et al. (2012) defined Mo and U enrichment factors of ~3–10 for suboxic conditions and > 10 for euxinic conditions. The Mo_{EF}/U_{EF} ratio further refines this distinction: values of 0.1–0.3 indicate oxic–suboxic conditions, 0.3–1.0 indicates anoxic conditions, and > 1.0 indicates sulfidic conditions (Algeo and Tribovillard, 2009; Hu et al., 2014).

Overall, Mo and U enrichments are generally more prominent and reliable indicators of redox conditions, but the degree of enrichment of other trace elements ultimately depends on specific depositional and diagenetic circumstances.

3.1.2 Trace element ratios as redox proxies

Element ratios are widely used as proxies to reconstruct paleo-redox environments. Ratios involving U, Th, V, Cr, Ni, and Co are widely applied to constrain redox states (Table 1). For example, Hatch and Leventhal (1992) proposed V/(V+Ni) as a proxy for evaluating paleoenvironmental and local redox conditions. Jones and Manning (1994) further evaluated five trace element ratios as potential redox proxies, including V/Cr, Ni/Co, Ni/V, (Cu+Mo)/Zn, and U/Th, though Ni/V and (Cu+Mo)/Zn were found to be less effective for ancient bottom water conditions. Building on this work, Algeo and Liu (2020) refined the application of trace-metal ratios in paleo-redox analysis. In general, ratios of U/Th > 1.25, V/Cr > 4.25, Ni/Co > 7.00, and V/(V+Ni) > 0.77 are considered indicative of suboxic and anoxic conditions. These proxies therefore provide important constraints on the redox state of the original sedimentary environment (Hatch and Leventhal, 1992; Jones and Manning, 1994; Pehlivanli et al., 2014; Chen et al., 2019).

The V/Sc ratio is another commonly applied redox proxy in paleoenvironmental studies (Kimura and Watanabe, 2001; Li et al., 2018), and some studies have linked it to methane seepage (Li et al., 2016; Sun et al., 2019). However, its ability to resolve redox shifts directly related to methane leakage is not always straightforward. Similarly, the Pr/Ph ratio has been used to differentiate anoxic (< 1.0), suboxic (1.0–3.0), and oxic (> 3.0) conditions (Jia, 2012), but it has rarely been used in gas hydrate-related studies.

To better explain the application of these proxies in gas hydrate-bearing sediment, we summarize case studies from four seep regions (Figure 4).

3.1.2.1 South China Sea

Shenhu samples contain a whole chimney and four chimney fragments, indicating more anoxic conditions during the core

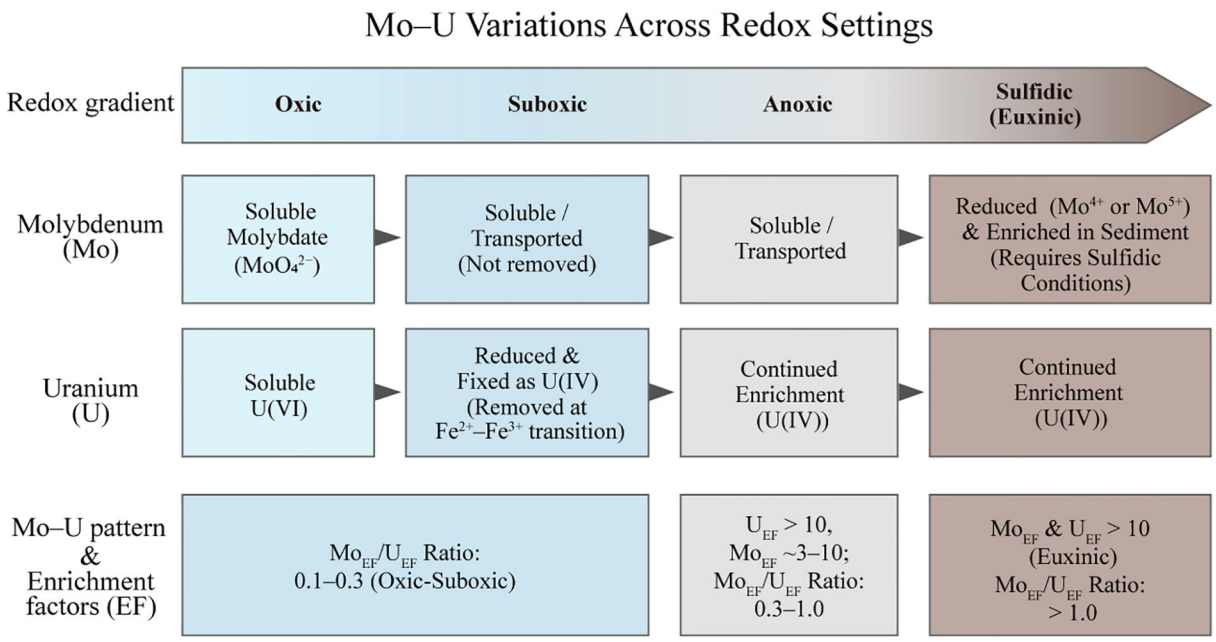

FIGURE 3
Schematic flow diagram illustrating the fractionation and enrichment mechanisms of Molybdenum (Mo) and Uranium (U) across marine sedimentary redox gradients. The diagram delineates the divergent behaviors of Mo and U under oxic, suboxic, and sulfidic (methane seep/euxinic) conditions. Mo enrichment (Mo_{EF} > 10) specifically requires free H_2S for thiomolybdate formation, whereas U enrichment begins under suboxic conditions. (Modified after Algeo and Tribovillard, 2009; Scott and Lyons, 2012).

formation stage under variable seepage (Ge et al., 2010). Dongsha chimneys, either scattered on the seafloor or protruding from sediments, likely precipitated from fluids that were influenced by surrounding sediments (Ge et al., 2010). At Qiongdongnan Site C14, cores recovered from a pockmark field show a shift from anoxic to suboxic conditions, reflecting methane leakage during deposition (Sun et al., 2019). Most samples from Shenhu and Dongsha have high U/Th and Ni/Co ratios, indicating anoxic conditions strongly influenced by active methane seepage and AOM. In particular, U/Th ratios in SH-HS4DG samples have a wide range, suggesting greatly varying methane fluid intensities. In contrast, Qiongdongnan samples reveal a predominantly oxic depositional environment, which may represent a weaker and more stable seepage activity.

3.1.2.2 Congo deep-sea fan

Carbonate from the Congo deep-sea fan (CF carbonates, Hu et al., 2014; GeoB carbonates, Feng et al., 2010), collected from pockmarks at Hydrate Hole and Diapir Field, formed under sulfidic conditions influenced by strong AOM and episodic H_2S release (Hu et al., 2014). Geochemical signatures indicate the pronounced effects of intense AOM and methane leakage: U/Th and Ni/Co ratios are consistent with oxygen-depleted conditions, whereas the wide range of V/Cr values suggests variability in methane leakage intensity.

3.1.2.3 Gulf of Mexico

Carbonates at site AC645 from the Gulf of Mexico show intermittent oxygenation during deposition, while carbonates at site GB425 from southern venting sites of a Gulf of Mexico mud volcano were affected by episodic methane leakage (Hu et al., 2014). AC645 samples exhibited polarized data, with some showing higher U/Th and Ni/Co values, indicating suboxic and anoxic conditions, pointing to intermittent methane emission. In contrast, GB425 carbonates show U/Th and Ni/Co values suggesting redox states fluctuating between oxic and dysoxic conditions, likely reflecting moderate methane seepage.

TABLE 1 Proxies of paleo-oxygenation.

Paleo-oxygenation facies	Oxygen concentration (ml/l)	U/Th	V/Cr	Ni/Co	V/(V+Ni)	Fe_{HR}/Fe_T
Oxic	8.0–2.0	< 0.75	< 2.00	< 5.00	< 0.60	< 0.22
Dysoxic	2.0–0.2	0.75–1.25	2.00–4.25	5.00–7.00	0.60–0.77	0.22–0.38
Suboxic and Anoxic	0.2–0.0 (sulfide present)	> 1.25	> 4.25	> 7.00	> 0.77	> 0.38

The limits for oxygen concentration are from Tyson and Pearson (1991). The limits for V/Cr, U/Th, and Ni/Co are from Jones and Manning (1994). The limits for V/(V+Ni) are from Hatch and Leventhal (1992). The limits for Fe_{HR}/Fe_T are from Poulton and Canfield (2011).

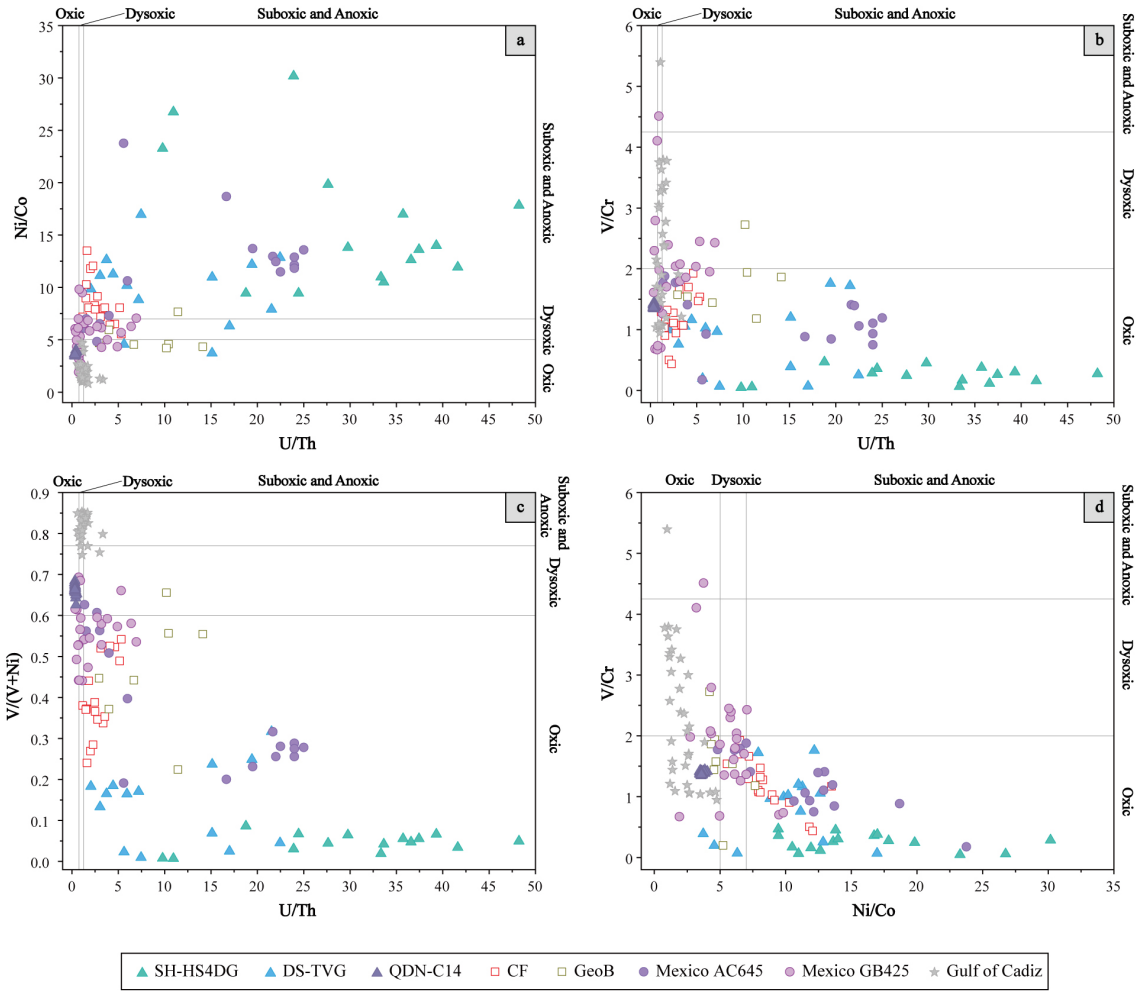

FIGURE 4
Application of U/Th, V/Cr, Ni/Co, and V/(V+Ni) ratios in cold seep carbonates and gas hydrate-bearing sediments. **(a)** U/Th *vs.* Ni/Co; **(b)** U/Th *vs.* V/Cr; **(c)** U/Th *vs.* V/(V+Ni); **(d)** Ni/Co *vs.* V/(V+Ni). 1, SH-HS4DG: carbonate chimney samples from Shenhu (data from Ge et al., 2010); 2, DS-TVG: sediment samples from Dongsha (data from Ge et al., 2010); 3, QDN-C14: Qiongdongnan sediments (data from Sun et al., 2019); 4, CF: carbonate samples from Congo deep-sea fan seep (data from Hu et al., 2014); 5, GeoB: carbonate samples from Congo deep-sea fan seep (data from Feng et al., 2010); 6, Mexico AC645 and GB425: carbonate samples from the Gulf of Mexico (data from Hu et al., 2014); 7, carbonate chimney samples from Gulf of Cadiz (data from Merinero Palomares et al., 2012). The limits for V/Cr, U/Th, and Ni/Co are from Jones and Manning (1994). The limits for V/(V+Ni) are from Hatch and Leventhal (1992).

3.1.2.4 Gulf of Cadiz

Carbonate chimneys from the Gulf of Cadiz formed under oxygen-depleted conditions associated with methane seepage and AOM (Merinero Palomares et al., 2012). These samples show relatively low U/Th and Ni/Co ratios, but elevated V/(V+Ni) ratios, indicating a hypoxic depositional environment. V/Cr ratios span wide ranges, oxic, dysoxic, suboxic, and anoxic stages, reflecting staged shifts in redox conditions linked to variable seepage intensity.

Despite their utility, trace element ratios can yield inconsistent results in modern sediments (Guo et al., 2021). Interpretations are often one-dimensional if they fail to account for seepage intensity and basin-wise geochemical baselines. Variations in seepage intensity can non-linearly alter redox zonations and element precipitation. For instance, V/Cr ratios in Gulf of Cadiz carbonates span multiple redox categories solely due to fluctuating seepage flux, while trace element contents in Congo Fan carbonates correlate directly with fluid flux periods. Furthermore, fixed redox thresholds are often inapplicable across different regions due to basin-specific trace elemental baselines. As emphasized by Algeo and Liu (2020), local depositional contexts determine background signals, necessitating internal cross-calibration rather than universal standards. Moreover, high seepage flux can compress redox zones, decoupling element precipitation from theoretical predictions (Li et al., 2024). Consequently, these ratios are best suited for tracking relative shifts in redox states rather than defining precise conditions, underscoring the necessity of a multi-proxy framework.

3.2 Speciation of iron and manganese

In marine sediments, Fe speciation is widely used to distinguish oxic, ferruginous, and euxinic water column conditions.

This approach has become central to reconstructing ocean redox chemistry (Table 1; Poulton and Canfield, 2011). Oxic conditions are typically defined by low ratios of highly reactive iron to total iron ($Fe_{HR}/Fe_T < 0.22$), while ferruginous conditions are indicated by $Fe_{HR}/Fe_T > 0.38$ and low ratios of pyrite iron to highly reactive iron ($Fe_{Py}/Fe_{HR} < 0.7–0.8$). Euxinic conditions are characterized by $Fe_{HR}/Fe_T > 0.38$ and $Fe_{Py}/Fe_{HR} > 0.7–0.8$, with values between 0.22 and 0.38 considered "equivocal". Sequential extraction procedures further characterize reactive iron pools—including carbonate-associated Fe (Fe_{Carb}), oxide Fe (Fe_{Ox}), and magnetite Fe (Fe_{Mag})—allowing for the evaluation of reactive iron cycling during methane seepage and diagenesis (Yang et al., 2018, 2023).

While manganese (Mn) geochemical behavior is often linked to iron, its role in methane cycling warrants distinct consideration due to its thermodynamic superiority (Slomp et al., 2013; Wu et al., 2020; Xue et al., 2025). Mn oxides serve as potent electron acceptors for anaerobic oxidation of methane (Mn-AOM), yielding significantly higher energy (approximately 20 times) than sulfate-driven AOM (Beal et al., 2009). This process proceeds via direct oxidation (MnR-AOM) or an indirect "cryptic sulfur cycle" (MnR-S-AOM), where Mn oxides recycle sulfide back to sulfate (Su et al., 2020; Cai et al., 2023; Xue et al., 2025). Geochemically, active Mn-AOM is signaled by elevated porewater Mn^{2+} concentrations below the SMTZ (Riedinger et al., 2014; Xiao et al., 2023). However, unlike Fe, Mn is extensively reduced to soluble Mn^{2+} in strongly reducing seep environments and tends to escape the sediment column, often leading to a net depletion of solid-phase Mn rather than authigenic accumulation (Nealson and Saffarini, 1994; Riedinger et al., 2014; Yang et al., 2018).

Iron (oxyhydr)oxides act as electron acceptors (Fe-AOM) following Mn depletion (Slomp et al., 2013; Egger et al., 2015). This process involves the direct coupling of methane oxidation with the reductive dissolution of crystalline Fe(III) oxides (Ettwig et al., 2016; Cai et al., 2018). In contrast to Mn, the liberated Fe^{2+} is more readily retained within the sediment through rapid reaction with HS^- and HCO_3^-, precipitating as authigenic Fe(II) carbonates (e.g., siderite) or sulfides (Slomp et al., 2013; Roberts, 2015; Yang et al., 2018, 2023). A unique signature in hydrocarbon-rich, sulfide-limited settings is the formation of ferrimagnetic iron sulfides, such as greigite (Fe_3S_4) and pyrrhotite, which serve as specific magnetic proxies for assessing seepage intensity (Roberts, 2015; Yang et al., 2023).

Collectively, the internal cycling of Mn and Fe drives the "benthic redox shuttle," facilitating the migration and enrichment of associated trace elements such as Mo, As, and V (Tribovillard et al., 2013; Hu et al., 2014; Smrzka et al., 2020). While both elements facilitate AOM, their distinct post-reduction fates—Mn export versus Fe retention—create diagnostic geochemical signatures crucial for reconstructing the history of fluid migration.

3.3 Elements related to organic matter

Redox states are closely linked to the distribution of organic carbon in sedimentary environments (Brumsack, 1989). Below the sulfate reduction zone, organic matter degradation drives methanogenesis (Johnson et al., 2014). Some studies have highlighted the relationship between total organic carbon (TOC) content and gas hydrate saturation (Waseda, 1998; Milkov, 2004; Johnson et al., 2014).

Authigenic barite minerals (e.g. $BaSO_4$) are almost insoluble and unaffected by redox conditions. They can form when sulfate diffuses downward below the seafloor and reacts with upward-migrating barium-rich fluids (Greinert et al., 2002). For this reason, biogenic barium (Ba) concentrations are commonly used as a proxy for past primary productivity on geological timescales (Dymond et al., 1992; McManus et al., 1998). In deep-sea sediments, Ca mainly originates from biogenic carbonates. A positive correlation between Ca and Ba is frequently observed (Emerson and Hedges, 2008; Carter et al., 2020; House and Norris, 2020).

In gas hydrate-bearing sediments, strong positive correlations between Ba and TOC or between Ba and Ca suggest that organic matter input exerts a key influence on Ba distribution (Merinero Palomares et al., 2012; Sun et al., 2019; Carter et al., 2020). This highlights the importance of organic carbon in regulating both redox states and mineral authigenesis in seep environments.

3.4 Rare earth element proxies

3.4.1 The total REE

REE accumulation is an important indicator of cold seep environments. REE concentrations in fresh water and seawater are generally very low (1–10 ng/L), with river water typically one order of magnitude higher than seawater (Yang and Li, 1999). Cold seep sediments, however, show REE enrichment compared to normal marine sediments (Figure 5a), largely due to early diagenesis (Freslon et al., 2014).

Ancient hydrocarbon seep studies show that ΣREE concentrations vary widely (0.3–43.7 ppm; Feng et al., 2009). Large variations have also been pointed out between surface, shallow, and bottom sediments from gas hydrate areas (Budakoglu et al., 2015). In cold seep sediments, ΣREE concentrations often increase at shallow depths but decrease at greater depths due to Fe-oxide reduction (Elderfield and Sholkovitz, 1987; Haley et al., 2004; Himmler et al., 2010). Cold seep carbonates (e.g., aragonite) formed during AOM can also act as sinks for REE. Rapid carbon deposition may dilute ΣREE concentrations, making decarbonation necessary before geochemical analysis (Wu et al., 2017; Liu et al., 2020). Furthermore, to minimize the influence of detrital input, normalization to TiO_2 ($\Sigma REE/TiO_2$) has been suggested (Tanaka et al., 2007).

3.4.2 REE patterns

Shale-normalized REE patterns provide insights into fluid sources and redox conditions. Modern seawater shows a characteristic pattern with a negative Ce anomaly, a positive La anomaly, and relative HREE enrichment (Feng et al., 2009; Ge et al., 2010; Himmler et al., 2010; Wang et al., 2018) (Figure 5a). In contrast, continental shelf sediments resemble river inputs,

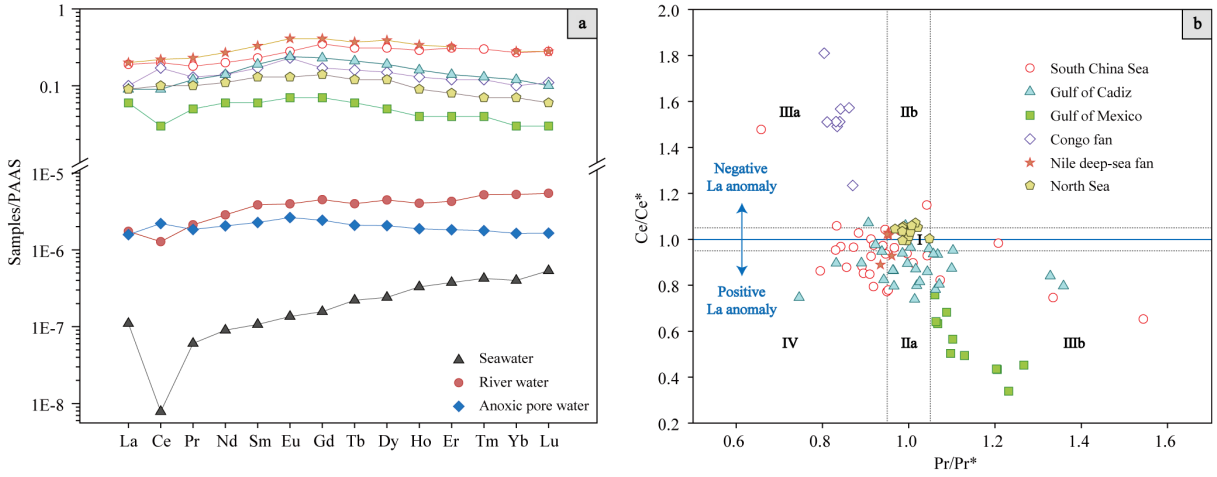

FIGURE 5
The distribution of REE in modern cold seep carbonates. **(a)** Average shale-normalized (PAAS; Taylor and McClennan, 1985) REE patterns for natural waters and modern cold seep carbonates from all over the world; **(b)** Plot of Ce/Ce* *vs.* Pr/Pr* after Bau and Dulski (1996) and Shields and Webb (2004). Ce/Ce* denotes $3Ce_N/(2La_N + Nd_N)$, and Pr/Pr* denotes $2Pr_N/(Ce_N + Nd_N)$, where N refers to normalization of concentration against the standard Post Archean Australian Shale (PAAS), Field I: no anomaly; Field IIa: positive La anomaly produces an apparent negative Ce anomaly; Field IIb: a negative La anomaly causes an apparent positive Ce anomaly; Field IIIa: real positive Ce anomaly; Field IIIb: real negative Ce anomaly; Field IV: positive La anomaly disguises a positive Ce anomaly. Data sources: 1. REE patterns of seawater, river water, and anoxic pore water are from Freslon et al. (2014); 2. the South China Sea (Wang et al., 2014); 3. Gulf of Cadiz (Wang et al., 2015); 4. Gulf of Mexico (Birgel et al., 2011); 5. Congo fan (Feng et al., 2010); 6. Nile deep-sea fan (Pierre et al., 2014); 7. North Sea (Crémière et al., 2016).

displaying flatter patterns with LREE enrichment, HREE depletion, and weak Ce and Eu anomalies (Piper, 1974; Goldstein and Jacobsen, 1988; Elderfield et al., 1990; Frimmel, 2009) (Figure 5a).

Cold seep carbonates worldwide generally show flat shale-normalized REE curves, slight Ce and Eu anomalies, MREE enrichment, and relative HREE depletion (Figure 5a). These patterns closely match the MREE-enriched signature of anoxic pore waters, suggesting that modern seep carbonates commonly precipitate under reducing conditions. Case studies from the South China Sea (Chen et al., 2005; Ge et al., 2010; Wang et al., 2014), Gulf of Cadiz (Wang et al., 2015), Gulf of Mexico (Feng et al., 2009; Birgel et al., 2011), Congo deep-sea fan (Feng et al., 2010), Niger delta (Rongemaille et al., 2011; Pierre et al., 2014), Makran accretionary prism (Himmler et al., 2010), North Sea (Crémière et al., 2016), and other seep sites confirm the use of REE patterns in tracking methane seepage, fluid sources, and precipitation conditions.

3.4.3 Cerium anomaly (Ce/Ce*)

Cerium (Ce) is the primary rare earth element that undergoes redox transformation in marine environment (Yang and Li, 1999). Ce(III) is readily oxidized to insoluble Ce(IV) and separates from other REE under oxidized and alkaline conditions, whereas in a reducing environment is reduced to soluble and is released from sediments to the pore water (Wright et al., 1987; Wilde et al., 1996). The Ce anomaly (Ce/Ce*) is thus a sensitive proxy for marine redox conditions. Historically, it was calculated as $Ce/Ce^* = 2Ce_N/(La_N + Pr_N)$ (Elderfield et al., 1990; Moffett, 1990). However, to avoid the influence of positive La anomalies common in seawater, the definition by Bau and Dulski (1996) is often preferred: $Ce/Ce^* = 3Ce_N/(2La_N + Nd_N)$, where N refers to normalization against PAAS or chondrite. Ce/Ce* ratios greater than 1.05 (a positive anomaly) indicate reducing conditions, while values below 0.95 (a negative anomaly) indicate oxic conditions (Taylor and McClennan, 1985). However, diagenetic modification is possible (Peckmann et al., 1999; Shields and Stille, 2001) and Ce anomalies are usually evaluated alongside Pr/Pr* (Bau and Dulski, 1996; Shields and Webb, 2004).

Cold seep carbonates display diverse Ce anomalies (Figure 5b). Positive Ce/Ce* anomalies in cold seep carbonates usually indicate the reducing conditions of gas hydrate-bearing anoxic environments (Feng and Chen, 2008; Feng et al., 2010; Birgel et al., 2011; Bian et al., 2012; Hu et al., 2014). For example, seep carbonates from the northern Congo fan display positive Ce anomalies ($Ce/Ce^* > 1.3$), suggesting precipitation under anoxic conditions (Feng et al., 2010). Conversely, negative Ce anomalies have been observed in seep carbonates from the Gulf of Mexico, and the Gulf of Cadiz, implying oxic conditions (Figure 5b). In contrast, samples from the South China Sea exhibit variable Ce anomalies (ranging from negative to positive), reflecting high spatial heterogeneity in redox environments. These negative anomalies may result from high alkalinity during AOM (Hu et al., 2014; Wu et al., 2017; Liu et al., 2020), organic-rich pore fluids (Pourret et al., 2008), or temporarily oxic conditions (Birgel et al., 2011; Bian et al., 2012). The coexistence of both negative and positive Ce anomalies within individual deposits reflects the spatial and temporal variability of seep redox environments (Wang et al., 2014, 2015).

4 Sedimentary proxies for methane seepage dynamics

4.1 Barite front

In the marine environment, Ba exists in dissolved and particulate forms (Chow and Goldberg, 1960), and predominantly precipitates as barite mineral (Liguori et al., 2016). Seafloor methane seepage is a major source of barite precipitation, as fluids released from gas hydrate decomposition or seepage are enriched in Ba^{2+} (Hu et al., 2014). This leads to higher Ba concentrations in bottom waters, where barite precipitates in surface sediments (Torres et al., 1996; Dickens, 2001; Torres et al., 2002; Feng and Chen, 2007; Vanneste et al., 2013). Barite formation is sensitive to pore water SO_4^{2-} concentrations. Barite cannot form below the SMTZ, where sulfate is fully exhausted (Dymond et al., 1992; Torres et al., 1996). With burial, barite deposited in sulfate-depleted zones dissolves and diffuses upwards as Ba^{2+} with migrating seep fluids. Upon encountering pore water sulfate above the SMTZ, barite re-precipitates, forming a distinct "barite front" (Figure 6; Torres et al., 1996; Dickens, 2001; Torres et al., 2003).

Global studies have shown that the barite front records long-term methane seepage activity. For example, Torres et al. (2003) systematically studied cold seep barite deposits across continental margins, while subsequent research in the Gulf of Mexico (Castellini et al., 2006; Feng and Roberts, 2011; Canet et al., 2014), San Clemente Basin (Torres et al., 2002), Storfjorden Trough (Yao et al., 2020), and the South China Sea (Liu et al., 2020), and ancient cold seeps (Gao et al., 2017) has revealed the geochemical coupling between Ba fluxes and CH_4 cycling.

The barite front is not static, as barite remineralization occurs due to the dynamic nature of seepage systems. A persistent barite front generally indicates stable hydrocarbon leakage that may persist for over 10^4 years (Torres et al., 1996; Feng and Chen, 2007). Ancient barite fronts can mark past SMTZ depths, thereby recording variations in methane flux over time. However, evidence of older fronts may be erased if the SMTZ shoals upward (Feng and Chen, 2007). Additionally, smaller Ba peaks may exist in the sedimentary profiles, possibly related to past episodes of enhanced (paleo)productivity (Dickens, 2001).

4.2 Molybdenum enrichment

The enrichment of Mo in marine sediments reflects its conservative behavior as molybdate in oxic seawater and its enhanced particle reactivity under sulfidic conditions (Scott and Lyons, 2012). Two main pathways have been identified: (i) transient enrichment related to Mn cycling near the sediment-water interface, and (ii) permanent enrichment in sulfidic environments where Mo is converted to thiomolybdates ($MoO_nS_{4-n}^{2-}$). The presence of free H_2S is therefore a key factor. In euxinic conditions, Mo concentrations typically exceed 60 ppm and may reach 100 ppm, whereas in H_2S-limited pore waters, values rarely exceed 25 ppm (Scott and Lyons, 2012).

Mo enrichments often highlight modern and paleo-SMTZs (Figure 6; Peketi et al., 2012; Pälike et al., 2014; Chen et al., 2016). Under strong cold seepage, the combination of AOM and SRB produces abundant H_2S, creating sulfidic conditions favorable for Mo enrichment (Niewöhner et al., 1998; Aharon and Fu, 2000; Joye et al., 2010). Extremely high Mo concentrations in sediments are therefore often interpreted as evidence for intense AOM-driven H_2S production (Peketi et al., 2012; Hu et al., 2014; Chen et al., 2016; Li et al., 2016; Liu et al., 2020).

Seepage strength influences the distribution of Mo. In weaker leakage systems, a deeper and wider SMTZ favors high-Mg calcite precipitation, with Mo enrichment spread across a broader sulfide zone (over vertical scales of meters or more) (Chen et al., 2016). Conversely, strong leakage leads to a shallower SMTZ (decimeter or centimeter depths) (Hu et al., 2015), compressing redox zones and favoring aragonite precipitation, bivalve survival, and Mo enrichment in surface sediments (Chen et al., 2016). Crucially, the extent of enrichment acts as a sensitive recorder of the sulfidization degree driven by seepage intensity (Scott and Lyons, 2012; Chen et al., 2016; Liu et al., 2020). In high-flux environments where dissolved sulfide concentrations exceed the threshold for quantitative thiomolybdate formation, Mo is efficiently scavenged and sequestered by iron sulfides (e.g., pyrite) or sulfurized organic matter, leading to extreme enrichments (Helz et al., 1996; Scott and Lyons, 2012; Chen et al., 2016; Li et al., 2018; Liu et al., 2020; Dai et al., 2025). Furthermore, the "benthic redox shuttle" significantly impacts Mo cycling by transporting adsorbed Mo—often enriched in light isotopes—from oxic waters to the sulfidic seep zone, where it is released upon reductive dissolution and subsequently fixed (Algeo and Tribovillard, 2009; Goldberg et al., 2009; Scott and Lyons, 2012; Hu et al., 2014; Jin et al., 2024; Miao et al., 2024b). Thus, combining concentration data with isotopic compositions provides a more robust constraint on the dynamic evolution of SMTZ and seepage history (Scott and Lyons, 2012; Chen et al., 2016; Miao et al., 2024b). U enrichment often parallels Mo, since high methane fluxes compress both suboxic and sulfidic zones, leading to U and Mo enrichment in shallow sediments.

4.3 Sr/Ca and Mg/Ca ratios

Within the SMTZ, AOM typically performed by a consortium of ANME and SRB, oxidizes large amounts of methane to HCO_3^- and reduces sulfate to HS^-. This process increases environmental alkalinity, leading to the precipitation of authigenic carbonate minerals such as low- and high-Mg calcite, dolomite, and aragonite (Ritger et al., 1987; Boetius et al., 2000). The key reaction is (Berner, 1980):

$$Ca^{2+} + 2HCO_3^- \rightarrow CaCO_3(s) + CO_2 + H_2O$$

Two main types of cold seep authigenic carbonates are aragonite and high-Mg calcite. Aragonite preferentially precipitates from seawater supersaturated in Mg^{2+} and Sr^{2+} (Berner, 1975; Tesoriero and Pankow, 1996), often in layers with free gas or close to gas hydrate horizons (Bohrmann et al., 1998;

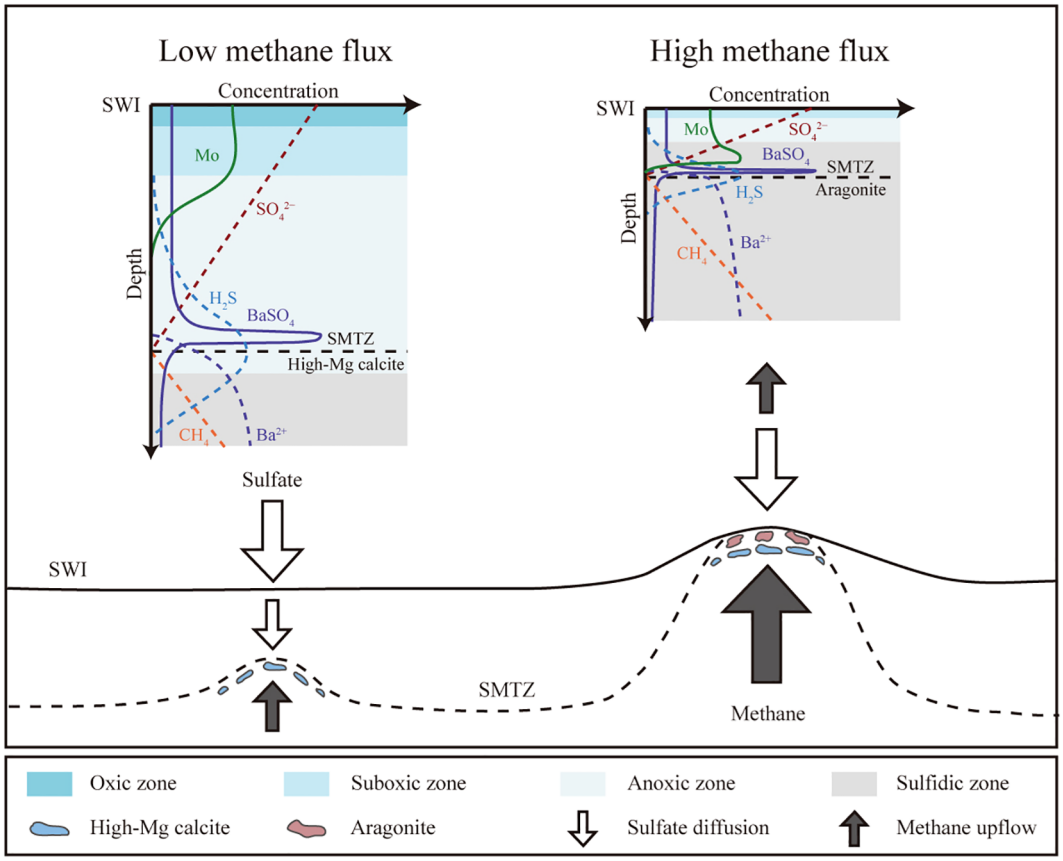

FIGURE 6
Schematic diagram of the formation of "barite front", enrichment of Mo, and types of authigenic carbonate under weak and strong seepage (Modified after Chen et al., 2016).

Naehr et al., 2000). High-Mg calcite, although less stable, preferentially precipitates under anoxic and low SO_4^{2-} conditions in methane seepage environments (Savard et al., 1996), especially within or below the sulfate reduction zone (Naehr et al., 2000; Greinert et al., 2001; Gieskes et al., 2005).

Because of their sensitivity to seepage intensity, Sr/Ca and Mg/Ca ratios are widely used to track fluid evolution (Bayon et al., 2007; Nöthen and Kasten, 2011; Yang et al., 2014; Chen et al., 2016; Sun et al., 2019; Liu et al., 2020). A four-endmember mixing model distinguishes between terrigenous input, biogenic calcite, aragonite (Sr-rich, reflecting strong seepage), and high-Mg calcite (linked to weak or diffusive seepage) (Bayon et al., 2007). For example, gas hydrate-bearing sediments from the South China Sea (Site GMGS2-W08) show a shift from high-Mg calcite to aragonite (Chen et al., 2016), reflecting a progressive increase in methane flux.

5 Distinct geochemical archives: differentiating signals in bulk sediments, authigenic carbonates, and pyrite

The core biogeochemical process in cold seep systems is SD-AOM, which generates HCO_3^- and H_2S. These byproducts promote the precipitation of authigenic carbonates and pyrite, significantly altering sedimentary redox conditions and thereby influencing the geochemical cycling of trace elements (Ritger et al., 1987; Peckmann et al., 2001; Sassen et al., 2004; Crémière et al., 2016; Miao et al., 2024b). While bulk sediment analysis provides an integrated record of these processes, the geochemical signatures recorded in specific sediment carriers differ significantly in their formation mechanisms and sensitivity to methane flux (Peckmann et al., 2001; Nöthen and Kasten, 2011; Liu et al., 2024; Dai et al., 2025) (Table 2).

5.1 Authigenic carbonates: direct records of methane-derived fluids

Unlike bulk sediments, which record a mixed signal of terrigenous input and authigenesis, authigenic carbonates, often referred to as methane-derived authigenic carbonates (MDAC), function as reliable archives of paleo-cold seep activity (Ritger et al., 1987; Bohrmann et al., 1998; Peckmann et al., 2001; Wilfert et al., 2015; Yao et al., 2020). The most diagnostic feature is the extremely negative authigenic carbonate $\delta^{13}C$ values (ranging from −60‰ to −30‰), typically ranging from −45.8‰ to −9.7‰ (Wang et al., 2015), or as low as −62.5‰ (Feng et al., 2010; Crémière et al., 2016), which confirm that the carbon source is

TABLE 2 Summary of distinct geochemical signatures and controlling mechanisms in different sediment carriers of cold seep systems.

Geochemical proxy	Authigenic carbonates (MDAC)	Authigenic pyrite	Bulk sediments
Inorganic Carbon ($\delta^{13}C$) & Oxygen ($\delta^{18}O$) Isotopes	$\delta^{13}C$: Highly negative (< −25‰, typically −60‰ to −30‰) due to incorporation of AOM-derived DIC. $\delta^{18}O$: Positive anomalies (e.g., +0.4‰ to +7.87‰) reflecting ^{18}O-rich fluids from gas hydrate dissociation. [Refs: Hesse and Harrison, 1981; Davidson et al., 1983; Ritger et al., 1987; Bohrmann et al., 1998; Aloisi et al., 2000; Peckmann and Thiel, 2004; Ussler and Paull, 2008; Wang et al., 2015; Crémière et al., 2016; Liu et al., 2020; Dai et al., 2025]	—	TIC: Elevated Total Inorganic Carbon (TIC) content with negative $\delta^{13}C_{TIC}$ values (< −5‰). Implication: Indicates the presence of dispersed authigenic carbonates within the sediment matrix. [Refs: Peketi et al., 2012; Li et al., 2024]
Sulfur Isotopes ($\delta^{34}S$) & Content	—	$\delta^{34}S$: Highly enriched values (up to +21‰). Mechanism: Closed-system Rayleigh distillation driven by high AOM rates enriches residual porewater in ^{34}S. [Refs: Jørgensen et al., 2004; Borowski et al., 2013; Sun et al., 2019; Chen et al., 2021]	Content: High Total Sulfur (TS) and TS/TOC ratios (> 0.36). Mechanism: Decoupled from organic carbon burial due to excess H_2S production from SD-AOM. [Refs: Miao et al., 2022; Liu et al., 2024]
Redox-Sensitive Elements	Enrichment: Mo, U, Ni, V, Cd, Co. Mechanism: Precipitation under anoxic/sulfidic porewater conditions. [Refs: Morford and Emerson, 1999; Algeo and Tribovillard, 2009; Hu et al., 2014; Wang et al., 2019; Smrzka et al., 2020]	Enrichment: Symbiotic Mo, As, and Fe. Mechanism: The "benthic Fe–Mn redox shuttle" transports Mo and As to the sulfidic zone, where they are captured by pyrite. [Refs: Tribovillard et al., 2013; Hu et al., 2014; Large et al., 2017; Miao et al., 2024b]	Mo/U: Co-enrichment (Mo_{EF} > 10) indicates compressed redox zones. W/Mn: Depletion (W_{EF}< 2) due to high solubility of thiotungstates and Mn diffusion. [Refs: Erickson and Helz, 2000; Algeo and Tribovillard, 2009; Chen et al., 2016; Miao et al., 2024a]
Metal Isotopes	—	$\delta^{98}Mo$ & $\delta^{56}Fe$: Isotopically light signatures (e.g., negative $\delta^{98}Mo$). Mechanism: Fractionation driven by the reductive dissolution of Fe–Mn oxides and subsequent capture by pyrite. [Refs: Goldberg et al., 2009; Fehr et al., 2010; Miao et al., 2024b]	Signal: Bulk measurements often reflect the light isotopic signatures of the authigenic pyrite fraction within the matrix. [Refs: Miao et al., 2024b]
Rare Earth Elements (REE)	Pattern: MREE enrichment (bulge). Ce Anomaly: Variable (positive/negative) depending on redox conditions and fluid source. [Refs: Haley et al., 2004; Himmler et al., 2010; Birgel et al., 2011; Wang et al., 2018; Smrzka et al., 2020]	—	Signal: Often diluted by terrigenous or biogenic components; authigenic REE signals may be less distinct than in pure carbonate phases. [Refs: Hu et al., 2014; Wang et al., 2014; Liu et al., 2020]
Mineralogy/ Morphology	Aragonite: High flux (High Sr/Ca). High-Mg Calcite: Low/Diffusive flux (High Mg/Ca). [Refs: Bayon et al., 2007; Li et al., 2024; Dai et al., 2025]	Framboidal: Characteristic of rapid formation under high sulfide flux conditions. [Refs: Peckmann et al., 2001; Merinero Palomares et al., 2012; Yang et al., 2023]	—

derived from the anaerobic oxidation of methane (biogenic or thermogenic) (Peckmann et al., 2001; Liu et al., 2020; Dai et al., 2025). Additionally, these carbonates typically exhibit positive $\delta^{18}O$ anomalies (e.g., +0.4‰ to +7.87‰) (Liu et al., 2020), reflecting the incorporation of $\delta^{18}O$-rich fluids released during gas hydrate dissociation (Bohrmann et al., 1998; Aloisi et al., 2000; Dai et al., 2025).

The mineralogical composition and elemental ratios of authigenic carbonates are highly sensitive to methane flux intensity (Nöthen and Kasten, 2011). High flux rates favor the precipitation of aragonite, characterized by high Sr/Ca ratios, whereas low or diffusive flux rates favor high-Mg calcite, indicated by high Mg/Ca ratios (Bayon et al., 2007; Nöthen and Kasten, 2011; Chen et al., 2016; Dai et al., 2025).

Regarding REE, authigenic carbonates often display a characteristic MREE bulge (enrichment in middle rare earth elements) (Himmler et al., 2010; Hu et al., 2014; Wang et al., 2018; Zhu et al., 2019), attributed to the reductive dissolution of Fe–Mn oxides in anoxic pore waters (Haley et al., 2004; Rongemaille et al., 2011; Crémière et al., 2016; Smrzka et al., 2020). The Ce anomaly varies with redox conditions: positive anomalies (Ce/Ce^* > 1) indicate strongly reducing environments (Feng et al., 2010; Wang et al., 2014; Zhu et al., 2019), while negative anomalies may reflect the influence of oxic seawater or specific diagenetic fluids (Algeo and Tribovillard,

2009; Feng et al., 2009; Birgel et al., 2011; Hu et al., 2014; Wang et al., 2019). Additionally, MDAC exhibit enrichment in redox-sensitive elements such as Mo, U, Ni, V, Cd, and Co (Hu et al., 2014; Wang et al., 2019; Smrzka et al., 2020), further demonstrating precipitation under anoxic conditions (Morford and Emerson, 1999; Algeo and Tribovillard, 2009). Therefore, the unique combination of isotopic, elemental, and mineralogical signatures makes MDAC a high-fidelity recorder, capable of documenting the intensity, duration, and fluid sources of past methane seepage.

5.2 Authigenic pyrite: redox and sulfur cycling proxies

Authigenic pyrite is formed when hydrogen sulfide (H_2S or HS^-) produced by SD-AOM reacts with Fe^{2+} (Berner, 1984; Ritger et al., 1987; Peckmann et al., 2001). The sulfur isotope ($\delta^{34}S$) composition of pyrite is a key indicator. High $\delta^{34}S$ values (up to +21‰) (Peketi et al., 2012; Li et al., 2016) suggest that the sulfate consumption rate exceeded the sulfate diffusion rate in a relatively closed system, leading to the enrichment of ^{34}S in the residual pore water pool, which is indicative of elevated methane flux (Jørgensen, 1979; Peketi et al., 2012; Borowski et al., 2013). Conversely, extremely negative $\delta^{34}S$ values (down to −51.0‰) (Peketi et al., 2012; Sun et al., 2019) can occur in environments with weak methane leakage, resulting in large sulfur isotope fractionation similar to that observed in OSR (Li et al., 2016). An abnormal enrichment of authigenic pyrite and high pyrite content (e.g., 1.77 to 10.45 wt%) (Miao et al., 2024b) coupled with ^{34}S enrichment is considered an effective indicator of methane seepage events (Peckmann et al., 2001; Jørgensen et al., 2004).

Pyrite also acts as a primary carrier for trace elements and other isotopes. Mo and As are often enriched and incorporated into the sediment concurrently with pyrite precipitation (Wang et al., 2019; Smrzka et al., 2020; Lin et al., 2021). This symbiotic enrichment is frequently linked to the "Fe–Mn shuttle process", which releases Fe, Mo, and As from Fe–Mn oxyhydroxides undergoing reductive dissolution in the deep euxinic environment (Tribovillard et al., 2013; Hu et al., 2014; Lin et al., 2021; Miao et al., 2024b). This process can also influence isotopic signatures: authigenic pyrite may record a relatively light Fe isotopic composition ($\delta^{56}Fe$ depletion) due to the reactivation of Fe (Miao et al., 2024b), and sediments may display a light $\delta^{98}Mo$ signature due to the release of light $\delta^{98}Mo$ from the reductive dissolution of Fe–Mn oxyhydroxides (Goldberg et al., 2009; Miao et al., 2024b).

5.3 Bulk sediments: integrated environmental signals

The geochemical signature of bulk sediment integrates the influence of SD-AOM on the sediment column and surrounding pore water (Liu et al., 2020). Methane seepage creates a strongly sulfidic environment, leading to the strong enrichment of Molybdenum (Mo) (Mo_{EF} > 10) (Algeo and Tribovillard, 2009; Chen et al., 2016; Miao et al., 2024b). A high Mo/W molar ratio (> 10) serves as a proxy for sulfidic environments characteristic of methane seepage, as Mo is sequestered as thiomolybdates (MoS_4^{2-}) (Erickson and Helz, 2000) while Tungsten (W) forms thiotungstates ($WO_nS_{4-n}^{2-}$) which are less readily buried, leading to W depletion (W_{EF}< 2) (Miao et al., 2024a). Additionally, Uranium (U) shows moderate to strong co-enrichment with Mo (Algeo and Tribovillard, 2009; Hu et al., 2015; Liu et al., 2020), suggesting that high methane fluxes compressed the suboxic (U enrichment zone) and sulfidic (Mo enrichment zone) zones into a narrow region (Morford and Emerson, 1999; Algeo and Tribovillard, 2009; Chen et al., 2016). Conversely, Manganese (Mn) is typically depleted due to the reductive dissolution of Fe–Mn oxyhydroxides and subsequent upward diffusion (Calvert and Pedersen, 1993; Goldberg et al., 2009; Pälike et al., 2014; Miao et al., 2024b).

Regarding bulk content, methane seepage environments feature elevated total sulfur (TS) content and a high TS/TOC ratio (Li et al., 2018; Miao et al., 2024a), deviating from normal marine ratios (Berner, 1984) due to the additional H_2S production from SD-AOM (Peketi et al., 2012; Miao et al., 2024b). Furthermore, elevated total inorganic carbon (TIC) content and negative $\delta^{13}C_{TIC}$ values (Liu et al., 2020; Miao et al., 2024a; Dai et al., 2025) indicate the presence of authigenic carbonates derived from AOM within the bulk sediment matrix (Li et al., 2024).

6 Summary

Gas hydrate-bearing and cold seep sediments exhibit distinctive geochemical characteristics, primarily driven by sulfate-methane interactions. These characteristics provide insights into both redox states and the temporal evolution of seepage activity.

- Globally, seepage-related carbonates and sediments are enriched in trace and rare earth elements (REE), acting as elemental reservoirs. Hypoxia is a common feature, as reflected by the enrichment of redox-sensitive elements (e.g., Mo, U, V, Ni, Cu) and shale-normalized REE patterns resembling anoxic pore waters. Nonetheless, localized oxidation events also occur, reflecting the episodic and dynamic nature of methane fluxes. Thus, while Mo and U are generally more prominent and reliable indicators, the degree of enrichment of all trace elements depends on local circumstances. In some cases, proxies such as negative Ce anomalies or lower U/Th, V/Cr, Ni/Co, and V/(V+Ni) ratios may signal temporary oxygenation.
- Reconstructing the history of seepage requires tracing SMTZ migration. Indicators include the barite front, Mo enrichment, and authigenic carbonate precipitation. Geochemical parameters (e.g., Sr/Ca and Mg/Ca ratios) can further provide additional constraints on seepage intensity. However, dynamic methane seepage often modifies earlier records, for example, through the dissolution of ancient barite fronts below a migrating SMTZ. Therefore, seepage reconstructions typically

require integration with pore water ion data and other supporting evidence.

- However, generalized interpretations of individual geochemical proxies are often insufficient. This review underscores the necessity of distinguishing among sedimentary carriers—bulk sediments, authigenic carbonates, and pyrite—to achieve reconstructions of methane seepage history. Geochemical signals are differentially partitioned among these phases: authigenic carbonates preserve high-fidelity records of fluid sources and methane flux intensity, whereas authigenic pyrite functions as a major sink for sulfur and chalcophile elements (e.g., Mo, As), recording sulfidization processes and benthic Fe–Mn redox shuttling. Decoupling these carrier-specific signals from the integrated bulk sediment record is essential to avoid misinterpretations caused by signal dilution or overprinting by background sedimentary inputs.

The effectiveness of inorganic geochemical proxies for characterizing methane-rich environments is well-established, but single-proxy approaches are insufficient. Instead, phase-specific multi-proxy frameworks are essential to capture the complex interplay among sediment sources, pore water chemistry, microbial processes, and methane fluxes. Finally, while this review has focused on elemental geochemistry, integrating isotopic approaches with conventional geochemical tools could provide complementary constraints on redox dynamics and methane cycling in future research.

Author contributions

YL: Investigation, Writing – review & editing, Writing – original draft, Methodology, Visualization. HY: Writing – review & editing, Methodology. YX: Writing – review & editing. YT: Writing – review & editing. CX: Writing – review & editing. HL: Conceptualization, Supervision, Writing – review & editing.

Funding

The author(s) declared that financial support was received for this work and/or its publication. This research is funded by DD20230400103 from China geological survey to HL, and National Natural Science Foundation of China (No. 42303075) to HY.

Conflict of interest

The author(s) declared that this work was conducted in the absence of any commercial or financial relationships that could be construed as a potential conflict of interest.

Generative AI statement

The author(s) declared that generative AI was not used in the creation of this manuscript.

Any alternative text (alt text) provided alongside figures in this article has been generated by Frontiers with the support of artificial intelligence and reasonable efforts have been made to ensure accuracy, including review by the authors wherever possible. If you identify any issues, please contact us.

Publisher's note

References

Aharon, P., and Fu, B. (2000). Microbial sulfate reduction rates and sulfur and oxygen isotope fractionations at oil and gas seeps in deepwater Gulf of Mexico. *Geochim. Cosmochim. Acta* 64, 233–246. doi: 10.1016/S0016-7037(99)00292-6

Algeo, T. J., and Liu, J. (2020). A re-assessment of elemental proxies for paleoredox analysis. *Chem. Geol.* 540, 119549. doi: 10.1016/j.chemgeo.2020.119549

Algeo, T. J., and Maynard, J. B. (2004). Trace-element behavior and redox facies in core shales of upper Pennsylvanian Kansas-type cyclothems. *Chem. Geol.* 206, 289–318. doi: 10.1016/j.chemgeo.2003.12.009

Algeo, T. J., and Tribovillard, N. (2009). Environmental analysis of paleoceanographic systems based on molybdenum–uranium covariation. *Chem. Geol.* 268, 211–225. doi: 10.1016/j.chemgeo.2009.09.001

Aloisi, G., Pierre, C., Rouchy, J. M., Foucher, J. P., and Woodside, J. (2000). Methane-related authigenic carbonates of eastern Mediterranean Sea mud volcanoes and their possible relation to gas hydrate destabilisation. *Earth Planet. Sci. Lett.* 184, 321–338. doi: 10.1016/S0012-821X(00)00322-8

Barnes, R. O., and Goldberg, E. D. (1976). Methane production and consumption in anoxic marine sediments. *Geology* 4, 297–300. doi: 10.1130/0091-7613(1976)42.0.CO;2

Barton, L. L., Goulhen, F., Bruschi, M., Woodards, N. A., Plunkett, R. M., and Rietmeijer, F. J. M. (2007). The bacterial metallome: Composition and stability with specific reference to the anaerobic bacterium *Desulfovibrio desulfuricans*. *Biometals* 20, 291–302. doi: 10.1007/s10534-006-9059-2

Bau, M., and Dulski, P. (1996). Distribution of yttrium and rare-earth elements in the Penge and Kuruman iron-formations, Transvaal Supergroup, South Africa. *Precambrian. Res.* 79, 37–55. doi: 10.1016/0301-9268(95)00087-9

Bayon, G., Pierre, C., Etoubleau, J., Voisset, M., Cauquil, E., Marsset, T., et al. (2007). Sr/Ca and Mg/Ca ratios in Niger Delta sediments: Implications for authigenic carbonate genesis in cold seep environments. *Mar. Geol.* 241, 93–109. doi: 10.1016/j.margeo.2007.03.007

Beal, E. J., House, C. H., and Orphan, V. J. (2009). Manganese- and iron-dependent marine methane oxidation. *Science* 325, 184–187. doi: 10.1126/science.1169984

Berner, R. A. (1975). The role of magnesium in the crystal growth of calcite and aragonite from sea water. *Geochim. Cosmochim. Acta* 39, 489–504. doi: 10.1016/0016-7037(75)90102-7

Berner, R. (1980). *Early diagenesis: A theoretical approach* (Princeton: Princeton University Press). doi: 10.1515/9780691209401

Berner, R. A. (1984). Sedimentary pyrite formation: an update. *Geochim. Cosmochim. Acta* 48, 605–615. doi: 10.1016/0016-7037(84)90089-9

Bian, Y. Y., Lin, Z. J., Feng, D., and Chen, D. F. (2012). Rare earth elements of seep carbonates and using them to trace redox variation at seep sites. *J. Trop. Oceanogr.* 31, 37–44. doi: 10.11978/j.issn.1009-5470.2012.05.006

Birgel, D., Feng, D., Roberts, H. H., and Peckmann, J. (2011). Changing redox conditions at cold seeps as revealed by authigenic carbonates from Alaminos Canyon, northern Gulf of Mexico. *Chem. Geol.* 285, 82–96. doi: 10.1016/j.chemgeo.2011.03.004

Björlykke, K. (1974). Geochemical and mineralogical influence of Ordovician Island Arcs on epicontinental clastic sedimentation. A study of Lower Palaeozoic sedimentation in the Oslo Region, Norway. *Sedimentology* 21, 251–272. doi: 10.1111/j.1365-3091.1974.tb02058.x

Boetius, A., Ravenschlag, K., Schubert, C. J., Rickert, D., Widdel, F., Gieseke, A., et al. (2000). A marine microbial consortium apparently mediating anaerobic oxidation of methane. *Nature* 407, 623–626. doi: 10.1038/35036572

Boetius, A., and Wenzhöfer, F. (2013). Seafloor oxygen consumption fuelled by methane from cold seeps. *Nat. Geosci.* 6, 725–734. doi: 10.1038/ngeo1926

Bohrmann, G., Greinert, J., Suess, E., and Torres, M. (1998). Authigenic carbonates from the Cascadia subduction zone and their relation to gas hydrate stability. *Geology* 26, 647–650. doi: 10.1130/0091-7613(1998)0262.3.CO;2

Borowski, W. S., Paull, C. K., and Ussler, W. III (1996). Marine pore-water sulfate profiles indicate in situ methane flux from underlying gas hydrate. *Geology* 24, 655–658. doi: 10.1130/0091-7613(1996)0242.3.CO;2

Borowski, W. S., Paull, C. K., and Ussler, W. (1999). Global and local variations of interstitial sulfate gradients in deep-water, continental margin sediments: Sensitivity to underlying methane and gas hydrates. *Mar. Geol.* 159, 131–154. doi: 10.1016/S0025-3227(99)00004-3

Borowski, W. S., Rodriguez, N. M., Paull, C. K., and Ussler, W. III (2013). Are ^{34}S-enriched authigenic sulfide minerals a proxy for elevated methane flux and gas hydrates in the geologic record? *Mar. Pet. Geol.* 43, 381–395. doi: 10.1016/j.marpetgeo.2012.12.009

Brumsack, H.-J. (1989). Geochemistry of recent TOC-rich sediments from the Gulf of California and the Black Sea. *Geol. Rundsch.* 78, 851–882. doi: 10.1007/BF01829327

Budakoglu, M., Abdelnasser, A., Karaman, M., and Kumral, M. (2015). The rare earth element geochemistry on surface sediments, shallow cores and lithological units of Lake Acıgöl Basin, Denizli, Turkey. *J. Asian Earth Sci.* 111, 632–662. doi: 10.1016/j.jseaes.2015.05.016

Cai, C., Leu, A. O., Xie, G.-J., Guo, J., Feng, Y., Zhao, J.-X., et al. (2018). A methanotrophic archaeon couples anaerobic oxidation of methane to Fe(III) reduction. *ISME. J.* 12, 1929–1939. doi: 10.1038/s41396-018-0109-x

Cai, C., Liu, D., Hu, Y., Huang, T., Jiang, Z., and Xu, C. (2023). Interlinked marine cycles of methane, manganese, and sulfate in the post-Marinoan Doushantuo cap dolostone. *Geochim. Cosmochim. Acta* 346, 245–258. doi: 10.1016/j.gca.2023.02.014

Caldwell, S. L., Laidler, J. R., Brewer, E. A., Eberly, J. O., Sandborgh, S. C., and Colwell, F. S. (2008). Anaerobic oxidation of methane: Mechanisms, bioenergetics, and the ecology of associated microorganisms. *Environ. Sci. Technol.* 42, 6791–6799. doi: 10.1021/es800120b

Calvert, S. E., and Pedersen, T. F. (1993). Geochemistry of Recent oxic and anoxic marine sediments: Implications for the geological record. *Mar. Geol.* 113, 67–88. doi: 10.1016/0025-3227(93)90150-T

Campbell, K. A. (2006). Hydrocarbon seep and hydrothermal vent paleoenvironments and paleontology: Past developments and future research directions. *Palaeogeogr. Palaeoclimatol. Palaeoecol.* 232, 362–407. doi: 10.1016/j.palaeo.2005.06.018

Canet, C., Anadón, P., González-Partida, E., Alfonso, P., Rajabi, A., Pérez-Segura, E., et al. (2014). Paleozoic bedded barite deposits from Sonora (NW Mexico): Evidence for a hydrocarbon seep environment of formation. *Ore. Geol. Rev.* 56, 292–300. doi: 10.1016/j.oregeorev.2013.06.009

Carter, S. C., Paytan, A., and Griffith, E. M. (2020). Toward an improved understanding of the marine barium cycle and the application of marine barite as a paleoproductivity proxy. *Minerals* 10, 421. doi: 10.3390/min10050421

Castellini, D. G., Dickens, G. R., Snyder, G. T., and Ruppel, C. D. (2006). Barium cycling in shallow sediment above active mud volcanoes in the Gulf of Mexico. *Chem. Geol.* 226, 1–30. doi: 10.1016/j.chemgeo.2005.08.008

Chen, F., Hu, Y., Feng, D., Zhang, X., Cheng, S., Cao, J., et al. (2016). Evidence of intense methane seepages from molybdenum enrichments in gas hydrate-bearing sediments of the northern South China Sea. *Chem. Geol.* 443, 173–181. doi: 10.1016/j.chemgeo.2016.09.029

Chen, D. F., Huang, Y. Y., Yuan, X. L., and Cathles, L. M. (2005). Seep carbonates and preserved methane oxidizing archaea and sulfate reducing bacteria fossils suggest recent gas venting on the seafloor in the Northeastern South China Sea. *Mar. Pet. Geol.* 22, 613–621. doi: 10.1016/j.marpetgeo.2005.05.002

Chen, T., Sun, X., Lin, Z., Lu, Y., Fang, Y., Wu, Z., et al. (2021). Deciphering the geochemical link between seep carbonates and enclosed pyrite: A case study from the northern South China Sea. *Mar. Pet. Geol.* 128, 105020. doi: 10.1016/j.marpetgeo.2021.105020

Chen, Y., Zhu, Z., and Zhang, L. (2019). Control actions of sedimentary environments and sedimentation rates on lacustrine oil shale distribution, an example of the oil shale in the Upper Triassic Yanchang Formation, southeastern Ordos Basin (NW China). *Mar. Pet. Geol.* 102, 508–520. doi: 10.1016/j.marpetgeo.2019.01.006

Chow, T. J., and Goldberg, E. D. (1960). On the marine geochemistry of barium. *Geochim. Cosmochim. Acta* 20, 192–198. doi: 10.1016/0016-7037(60)90073-9

Chun, C. O. J., Delaney, M. L., and Zachos, J. C. (2010). Paleoredox changes across the Paleocene-Eocene Thermal Maximum, Walvis Ridge (ODP sites 1262, 1263, and 1266): Evidence from Mn and U enrichment factors. *Paleoceanography* 25. doi: 10.1029/2009PA001861

Consolaro, C., Rasmussen, T. L., Panieri, G., Mienert, J., Bünz, S., and Sztybor, K. (2015). Carbon isotope (δ^{13}C) excursions suggest times of major methane release during the last 14 kyr in Fram Strait, the deep-water gateway to the Arctic. *Clim. Past.* 11, 669–685. doi: 10.5194/cp-11-669-2015

Crémière, A., Bayon, G., Ponzevera, E., and Pierre, C. (2013). Paleo-environmental controls on cold seep carbonate authigenesis in the Sea of Marmara. *Earth Planet. Sci. Lett.* 376, 200–211. doi: 10.1016/j.epsl.2013.06.029

Crémière, A., Lepland, A., Chand, S., Sahy, D., Kirsimäe, K., Bau, M., et al. (2016). Fluid source and methane-related diagenetic processes recorded in cold seep carbonates from the Alvheim Channel, central North Sea. *Chem. Geol.* 432, 16–33. doi: 10.1016/j.chemgeo.2016.03.019

Cui, H., Su, X., Chen, F., Holland, M., Yang, S., Liang, J., et al. (2019). Microbial diversity of two cold seep systems in gas hydrate-bearing sediments in the South China Sea. *Mar. Environ. Res.* 144, 230–239. doi: 10.1016/j.marenvres.2019.01.009

Dai, K., Miao, X., Gu, Y., Chang, X., Li, Q., Zhuang, G., et al. (2025). Cold-seep carbonate factory: Formation mechanisms, geochemical proxies, and implications for global carbon cycling. *J. Ocean. Univ. China*., 1–18. doi: 10.1007/s11802-026-6261-4

Davidson, D. W., Leaist, D. J., and Hesse, R. (1983). Oxygen-18 enrichment in water of a clathrate hydrate. *Geochim. Cosmochim. Acta* 47, 2293–2295. doi: 10.1016/0016-7037(83)90053-4

Deng, Y. N., Fang, Y. X., Zhang, X., Chen, F., Wang, H. F., Ren, J. B., et al. (2017). Trace element geochemistry of sediments in the Qiongdongnan area, the South China Sea, and its implications for gas hydrates. *Mar. Geol. Quat. Geol.* 37, 70–81. doi: 10.16562/j.cnki.0256-1492.2017.05.007

Devol, A. H., and Ahmed, S. I. (1981). Are high rates of sulphate reduction associated with anaerobic oxidation of methane? *Nature* 291, 407–408. doi: 10.1038/291407a0

Dickens, G. R. (2001). Sulfate profiles and barium fronts in sediment on the Blake Ridge: Present and past methane fluxes through a large gas hydrate reservoir. *Geochim. Cosmochim. Acta* 65, 529–543. doi: 10.1016/S0016-7037(00)00556-1

Dymond, J., Suess, E., and Lyle, M. (1992). Barium in deep-sea sediment: A geochemical proxy for paleoproductivity. *Paleoceanography* 7, 163–181. doi: 10.1029/92PA00181

Egger, M., Rasigraf, O., Sapart, C. J., Jilbert, T., Jetten, M. S. M., Röckmann, T., et al. (2015). Iron-mediated anaerobic oxidation of methane in brackish coastal sediments. *Environ. Sci. Technol.* 49, 277–283. doi: 10.1021/es503663z

Egger, M., Riedinger, N., Mogollón, J. M., and Jørgensen, B. B. (2018). Global diffusive fluxes of methane in marine sediments. *Nat. Geosci.* 11, 421–425. doi: 10.1038/s41561-018-0122-8

Elderfield, H., and Sholkovitz, E. R. (1987). Rare earth elements in the pore waters of reducing nearshore sediments. *Earth Planet. Sci. Lett.* 82, 280–288. doi: 10.1016/0012-821X(87)90202-0

Elderfield, H., Upstill-Goddard, R., and Sholkovitz, E. R. (1990). The rare earth elements in rivers, estuaries, and coastal seas and their significance to the composition of ocean waters. *Geochim. Cosmochim. Acta* 54, 971–991. doi: 10.1016/0016-7037(90)90432-K

Emerson, S., and Hedges, J. (2008). *Chemical oceanography and the marine carbon cycle* (Cambridge: Cambridge University Press). doi: 10.1017/CBO9780511793202

Erickson, B. E., and Helz, G. R. (2000). Molybdenum (VI) speciation in sulfidic waters: stability and lability of thiomolybdates. *Geochim. Cosmochim. Acta* 64, 1149–1158. doi: 10.1016/S0016-7037(99)00423-8

Ettwig, K. F., Zhu, B., Speth, D., Keltjens, J. T., Jetten, M. S. M., and Kartal, B. (2016). Archaea catalyze iron-dependent anaerobic oxidation of methane. *Proc. Natl. Acad. Sci.* 113, 12792–12796. doi: 10.1073/pnas.1609534113

Fehr, M. A., Andersson, P. S., Halenius, U., Gustafsson, O., and Morth, C.-M. (2010). Iron enrichments and Fe isotopic compositions of surface sediments from the Gotland deep, Baltic Sea. *Chem. Geol.* 277, 310–322. doi: 10.1016/j.chemgeo.2010.08.014

Feng, D., and Chen, D. F. (2007). Barium cycling in pore water of seafloor sediment: Indicator of methane fluxes. *Adv. Earth Sci.* 22, 49–57. doi: 10.11867/j.issn.1001-8166.2007.01.0049

Feng, D., and Chen, D. F. (2008). Petrographic characterization and rare earth elements as geochemical tracers for redox condition of seep carbonates from northwestern Black Sea. *Geoscience* 22, 390–396. doi: 10.3969/j.issn.1000-8527.2008.03.007

Feng, D., Chen, D., and Peckmann, J. (2009). Rare earth elements in seep carbonates as tracers of variable redox conditions at ancient hydrocarbon seeps. *Terra. Nova.* 21, 49–56. doi: 10.1111/j.1365-3121.2008.00855.x

Feng, D., Chen, D., Peckmann, J., and Bohrmann, G. (2010). Authigenic carbonates from methane seeps of the northern Congo Fan: Microbial formation mechanism. *Mar. Pet. Geol.* 27, 748–756. doi: 10.1016/j.marpetgeo.2009.08.006

Feng, D., and Roberts, H. H. (2011). Geochemical characteristics of the barite deposits at cold seeps from the northern Gulf of Mexico continental slope. *Earth Planet. Sci. Lett.* 309, 89–99. doi: 10.1016/j.epsl.2011.06.017

Francois, R. (1988). A study on the regulation of the concentrations of some trace metals (Rb C.OMMAS.R.X.X.X, Zn, Pb, Cu, V, Cr, Ni, Mn and Mo) in Saanich Inlet

sediments, British Columbia, Canada. *Mar. Geol.* 83, 285–308. doi: 10.1016/0025-3227(88)90063-1

Freslon, N., Bayon, G., Toucanne, S., Bermell, S., Bollinger, C., Chéron, S., et al. (2014). Rare earth elements and neodymium isotopes in sedimentary organic matter. *Geochim. Cosmochim. Acta* 140, 177–198. doi: 10.1016/j.gca.2014.05.016

Frimmel, H. E. (2009). Trace element distribution in Neoproterozoic carbonates as palaeoenvironmental indicator. *Chem. Geol.* 258, 338–353. doi: 10.1016/j.chemgeo.2008.10.033

Froelich, P. N., Klinkhammer, G. P., Bender, M. L., Luedtke, N. A., Heath, G. R., Cullen, D., et al. (1979). Early oxidation of organic matter in pelagic sediments of the eastern equatorial Atlantic: Suboxic diagenesis. *Geochim. Cosmochim. Acta* 43, 1075–1090. doi: 10.1016/0016-7037(79)90095-4

Gao, J., Yang, R., Chen, J., Zheng, L., Cheng, W., and Wei, H. (2017). Multiple proxies indicating methane seepage as the origin of Devonian large barite deposit in Zhenning-Ziyun, Guizhou, SW China. *Ore. Geol. Rev.* 80, 18–26. doi: 10.1016/j.oregeorev.2016.06.020

Ge, L., Jiang, S.-Y., Swennen, R., Yang, T., Yang, J.-H., Wu, N.-Y., et al. (2010). Chemical environment of cold seep carbonate formation on the northern continental slope of South China Sea: Evidence from trace and rare earth element geochemistry. *Mar. Geol.* 277, 21–30. doi: 10.1016/j.margeo.2010.08.008

Gieskes, J., Mahn, C., Day, S., Martin, J. B., Greinert, J., Rathburn, T., et al. (2005). A study of the chemistry of pore fluids and authigenic carbonates in methane seep environments: Kodiak Trench, Hydrate Ridge, Monterey Bay, and Eel River Basin. *Chem. Geol.* 220, 329–345. doi: 10.1016/j.chemgeo.2005.04.002

Glass, J. B., Chen, S., Dawson, K. S., Horton, D. R., Vogt, S., Ingall, E. D., et al. (2017). Trace metal imaging of sulfate-reducing bacteria and methanogenic archaea at single-cell resolution by synchrotron X-ray fluorescence imaging. *Geomicrobiol. J.* 35, 81–89. doi: 10.1080/01490451.2017.1321068

Glass, J. B., and Orphan, V. J. (2012). Trace metal requirements for microbial enzymes involved in the production and consumption of methane and nitrous oxide. *Front. Microbiol.* 3. doi: 10.3389/fmicb.2012.00061

Glass, J. B., Yu, H., Steele, J. A., Dawson, K. S., Sun, S., Chourey, K., et al. (2014). Geochemical, metagenomic and metaproteomic insights into trace metal utilization by methane-oxidizing microbial consortia in sulphidic marine sediments. *Environ. Microbiol.* 16, 1592–1611. doi: 10.1111/1462-2920.12314

Goldberg, T., Archer, C., Vance, D., and Poulton, S. W. (2009). Mo isotope fractionation during adsorption to Fe (oxyhydr) oxides. *Geochim. Cosmochim. Acta.* 73, 6502–6516. doi: 10.1016/j.gca.2009.08.004

Goldhaber, M. B. (2003). "7.10 - sulfur-rich sediments," in *Treatise on Geochemistry*. Eds. H. D. Holland and K. K. Turekian (Pergamon, Oxford), 257–288. doi: 10.1016/B0-08-043751-6/07139-5

Goldstein, S. J., and Jacobsen, S. B. (1988). Rare earth elements in river waters. *Earth Planet. Sci. Lett.* 89, 35–47. doi: 10.1016/0012-821X(88)90031-3

Greinert, J., Bohrmann, G., and Suess, E. (2001). "Gas hydrate-associated carbonates and methane-venting at Hydrate Ridge: Classification, distribution, and origin of authigenic lithologies," in *Natural Gas Hydrates: Occurrence, Distribution, and Detection* (Washington, DC, United States: American Geophysical Union (AGU), 99–113. doi: 10.1029/GM124p0099

Greinert, J., Bollwerk, S. M., Derkachev, A., Bohrmann, G., and Suess, E. (2002). Massive barite deposits and carbonate mineralization in the Derugin Basin, Sea of Okhotsk: Precipitation processes at cold seep sites. *Earth Planet. Sci. Lett.* 203, 165–180. doi: 10.1016/S0012-821X(02)00830-0

Griffith, E. M., and Paytan, A. (2012). Barite in the ocean – occurrence, geochemistry and palaeoceanographic applications. *Sedimentology* 59, 1817–1835. doi: 10.1111/j.1365-3091.2012.01327.x

Guo, W., Chen, G., Li, Y., Li, Y., Zhang, Y., Zhou, J., et al. (2021). Factors controlling the lower radioactivity and its relation with higher organic matter content for Middle Jurassic Oil Shale in Yuqia Depression, Northern Qaidam Basin, China: Evidence from Organic and Inorganic Geochemistry. *ACS Omega.* 6, 7360–7373. doi: 10.1021/acsomega.0c05618

Haley, B. A., Klinkhammer, G. P., and McManus, J. (2004). Rare earth elements in pore waters of marine sediments. *Geochim. Cosmochim. Acta* 68, 1265–1279. doi: 10.1016/j.gca.2003.09.012

Hatch, J. R., and Leventhal, J. S. (1992). Relationship between inferred redox potential of the depositional environment and geochemistry of the Upper Pennsylvanian (Missourian) Stark Shale Member of the Dennis Limestone, Wabaunsee County, Kansas, U.S.A. *Chem. Geol.* 99, 65–82. doi: 10.1016/0009-2541(92)90031-Y

Helz, G. R., Miller, C. V., Charnock, J. M., Mosselmans, J. F. W., Pattrick, R. A. D., Garner, C. D., et al. (1996). Mechanism of molybdenum removal from the sea and its concentration in black shales: EXAFS evidence. *Geochim. Cosmochim. Acta* 60, 3631–3642. doi: 10.1016/0016-7037(96)00195-0

Hesse, R., and Harrison, W. E. (1981). Gas hydrates (clathrates) causing pore-water freshening and oxygen isotope fractionation in deep-water sedimentary sections of terrigenous continental margins. *Earth Planet. Sci. Lett.* 55, 453–462. doi: 10.1016/0012-821X(81)90172-2

Himmler, T., Bach, W., Bohrmann, G., and Peckmann, J. (2010). Rare earth elements in authigenic methane-seep carbonates as tracers for fluid composition during early diagenesis. *Chem. Geol.* 277, 126–136. doi: 10.1016/j.chemgeo.2010.07.015

Hinrichs, K.-U., and Boetius, A. (2003). "The anaerobic oxidation of methane: New insights in microbial ecology and biogeochemistry," in *Ocean Margin Systems*. Eds. G. Wefer, D. Billett, D. Hebbeln, B. B. Jørgensen, M. Schlüter and T.C.E.v. Weering (Springer, Berlin, Heidelberg), 457–477. doi: 10.1007/978-3-662-05127-6_28

Hiruta, A., Snyder, G. T., Tomaru, H., and Matsumoto, R. (2009). Geochemical constraints for the formation and dissociation of gas hydrate in an area of high methane flux, eastern margin of the Japan Sea. *Earth Planet. Sci. Lett.* 279, 326–339. doi: 10.1016/j.epsl.2009.01.015

House, B. M., and Norris, R. D. (2020). Unlocking the barite paleoproductivity proxy: A new high-throughput method for quantifying barite in marine sediments. *Chem. Geol.* 552, 119664. doi: 10.1016/j.chemgeo.2020.119664

Hu, Y., Feng, D., Liang, Q., Xia, Z., Chen, L., and Chen, D. (2015). Impact of anaerobic oxidation of methane on the geochemical cycle of redox-sensitive elements at cold-seep sites of the northern South China Sea. *Deep. Sea. Res. Part II.* 122, 84–94. doi: 10.1016/j.dsr2.2015.06.012

Hu, Y., Feng, D., Peckmann, J., Roberts, H. H., and Chen, D. (2014). New insights into cerium anomalies and mechanisms of trace metal enrichment in authigenic carbonate from hydrocarbon seeps. *Chem. Geol.* 381, 55–66. doi: 10.1016/j.chemgeo.2014.05.014

Huerta-Diaz, M. A., and Morse, J. W. (1990). A quantitative method for determination of trace metal concentrations in sedimentary pyrite. *Mar. Chem.* 29, 119–144. doi: 10.1016/0304-4203(90)90009-2

Jia, J. (2012). *Research on the recognition and resource evaluation of the Upper Cretaceous oil shale based on geochemistry-geophysics technique in the Songliao Basin (NE, China)* (Changchun, China: Jilin University). doi: 10.13140/RG.2.2.25683.30243

Jin, M., Chen, F., Li, N., Peckmann, J., Mathur, R., Godfrey, L., et al. (2024). Isotope evidence for the enrichment mechanism of molybdenum in methane-seep sediments: Implications for past seepage intensity. *Geochim. Cosmochim. Acta* 373, 282–291. doi: 10.1016/j.gca.2024.04.003

Johnson, J. E., Phillips, S. C., Torres, M. E., Piñero, E., Rose, K. K., and Giosan, L. (2014). Influence of total organic carbon deposition on the inventory of gas hydrate in the Indian continental margins. *Mar. Pet. Geol.* 58, 406–424. doi: 10.1016/j.marpetgeo.2014.08.021

Jones, B., and Manning, D. A. C. (1994). Comparison of geochemical indices used for the interpretation of palaeoredox conditions in ancient mudstones. *Chem. Geol.* 111, 111–129. doi: 10.1016/0009-2541(94)90085-X

Jørgensen, B. B. (1979). A theoretical model of the stable sulfur isotope distribution in marine sediments. *Geochim. Cosmochim. Acta* 43, 363–374. doi: 10.1016/0016-7037(79)90201-1

Jørgensen, B. B., Böttcher, M. E., Lüschen, H., Neretin, L., and Volkov, I. (2004). Anaerobic methane oxidation and a deep H_2S sink generate isotopically heavy sulfides in Black Sea sediments. *Geochim. Cosmochim. Acta* 68, 2095–2118. doi: 10.1016/j.gca.2003.07.017

Jørgensen, B. B., and Kasten, S. (2006). "Sulfur cycling and methane oxidation," in *Marine Geochemistry*. Eds. H. D. Schulz and M. Zabel (Springer, Berlin, Heidelberg), 271–309. doi: 10.1007/3-540-32144-6_8

Joye, S. B., Boetius, A., Orcutt, B. N., Montoya, J. P., Schulz, H. N., Erickson, M. J., et al. (2004). The anaerobic oxidation of methane and sulfate reduction in sediments from Gulf of Mexico cold seeps. *Chem. Geol.* 205, 219–238. doi: 10.1016/j.chemgeo.2003.12.019

Joye, S. B., Bowles, M. W., Samarkin, V. A., Hunter, K. S., and Niemann, H. (2010). Biogeochemical signatures and microbial activity of different cold-seep habitats along the Gulf of Mexico deep slope. *Deep. Sea. Res. Part II.* 57, 1990–2001. doi: 10.1016/j.dsr2.2010.06.001

Kimura, H., and Watanabe, Y. (2001). Oceanic anoxia at the Precambrian-Cambrian boundary. *Geology* 29, 995. doi: 10.1130/0091-7613(2001)0292.0.CO;2

Knittel, K., and Boetius, A. (2009). Anaerobic oxidation of methane: Progress with an unknown process. *Annu. Rev. Microbiol.* 63, 311–334. doi: 10.1146/annurev.micro.61.080706.093130

Kong, Y., Lei, H., Zhang, Z., Cheng, W., Wang, B., Pan, F., et al. (2021). Depth profiles of geochemical features, geochemical activities and biodiversity of microbial communities in marine sediments from the Shenhu area, the northern South China Sea. *Sci. Total. Environ.* 779, 146233. doi: 10.1016/j.scitotenv.2021.146233

Large, R. R., Mukherjee, I., Gregory, D. D., Steadman, J. A., Maslennikov, V. V., and Meffre, S. (2017). Ocean and atmosphere geochemical proxies derived from trace elements in marine pyrite: Implications for ore genesis in sedimentary basins. *Econ. Geol.* 112, 423–450. doi: 10.2113/econgeo.112.2.423

Li, N., Feng, D., Chen, L., Wang, H., and Chen, D. (2016). Using sediment geochemistry to infer temporal variation of methane flux at a cold seep in the South China Sea. *Mar. Pet. Geol.* 77, 835–845. doi: 10.1016/j.marpetgeo.2016.07.026

Li, J., Li, L., Bai, S., Ta, K., Xu, H., Chen, S., et al. (2019). New insight into the biogeochemical cycling of methane, S and Fe above the sulfate-methane transition zone in methane hydrate-bearing sediments: A case study in the Dongsha area, South China Sea. *Deep. Sea. Res. Part I.* 145, 97–108. doi: 10.1016/j.dsr.2019.01.011

Li, J., Tang, S., Zhang, S., Xi, Z., Yang, N., Yang, G., et al. (2018). Paleo-environmental conditions of the Early Cambrian Niutitang Formation in the Fenggang area, the southwestern margin of the Yangtze Platform, southern China: Evidence from major elements, trace elements and other proxies. *J. Asian Earth Sci.* 159, 81–97. doi: 10.1016/j.jseaes.2018.03.013

Li, Q., Wang, H., Cai, F., Luo, D., Kong, F., Li, A., et al. (2024). Influence of methane seep activities and sea-level changes on elemental and isotopic compositions and abundance of carbonates in sediments of the Okinawa Trough since the last glacial period. *J. Asian Earth Sci.* 260, 105942. doi: 10.1016/j.jseaes.2023.105942

Liguori, B. T. P., Almeida, M. G. D., and Rezende, C. E. D. (2016). Barium and its importance as an indicator of (paleo)productivity. *An. Acad. Bras. Ciênc.* 88, 2093–2103. doi: 10.1590/0001-3765201620140592

Lin, Z., Sun, X., Strauss, H., Eroglu, S., Böttcher, M. E., Lu, Y., et al. (2021). Molybdenum isotope composition of seep carbonates – constraints on sediment biogeochemistry in seepage environments. *Geochim. Cosmochim. Acta* 307, 56–71. doi: 10.1016/j.gca.2021.05.038

Liu, S., Feng, X., Feng, Z., Xiao, X., and Feng, L. (2020). Geochemical evidence of methane seepage in the sediments of the Qiongdongnan Basin, South China Sea. *Chem. Geol.* 543, 119588. doi: 10.1016/j.chemgeo.2020.119588

Liu, X., Wang, H., Liu, J., and Zhuang, G.-C. (2024). Microbial sulfate reduction and its role in carbon sequestration in marine sediments. *J. Earth Sci.* 35, 1378–1381. doi: 10.1007/s12583-024-1998-4

McManus, J., Berelson, W. M., Klinkhammer, G. P., Johnson, K. S., Coale, K. H., Anderson, R. F., et al. (1998). Geochemistry of barium in marine sediments: Implications for its use as a paleoproxy. *Geochim. Cosmochim. Acta* 62, 3453–3473. doi: 10.1016/S0016-7037(98)00248-8

McQuay, E. L., Torres, M. E., Collier, R. W., Huh, C.-A., and McManus, J. (2008). Contribution of cold seep barite to the barium geochemical budget of a marginal basin. *Deep. Sea. Res. Part I.* 55, 801–811. doi: 10.1016/j.dsr.2008.03.001

Merinero Palomares, R., Lunar Hernández, R., and Martínez Frías, J. (2012). Mechanisms of trace metal enrichment in submarine, methane-derived carbonate chimneys from the Gulf of Cadiz. *J. Geochem. Explor.* 112, 297–305. doi: 10.1016/j.gexplo.2011.09.011

Miao, X., Liu, X., Li, Q., Li, A., Cai, F., Kong, F., et al. (2022). Porewater geochemistry indicates methane seepage in the Okinawa Trough and its implications for the carbon cycle of the Subtropical West Pacific. *Palaeogeogr. Palaeoclimatol. Palaeoecol.* 607, 111266. doi: 10.1016/j.palaeo.2022.111266

Miao, X., Oppo, D., Wei, J., Lin, Z., Liu, X., Wu, T., et al. (2024a). Enrichment pattern of tungsten in sediments under methane seepage environments: Applicability as a proxy for tracing and reconstructing (paleo-)methane seepage. *Chem. Geol.* 663, 122262. doi: 10.1016/j.chemgeo.2024.122262

Miao, X., Wei, J., Li, J., Liu, X., Wang, D., Li, J., et al. (2024b). Isotopically light Mo in sediments of methane seepage controlled by the benthic Fe–Mn redox shuttle process. *Glob. Planet. Change* 239, 104512. doi: 10.1016/j.gloplacha.2024.104512

Milkov, A. V. (2004). Global estimates of hydrate-bound gas in marine sediments: How much is really out there? *Earth Sci. Rev.* 66, 183–197. doi: 10.1016/j.earscirev.2003.11.002

Moffett, J. W. (1990). Microbially mediated cerium oxidation in sea water. *Nature* 345, 421–423. doi: 10.1038/345421a0

Morford, J. L., and Emerson, S. (1999). The geochemistry of redox sensitive trace metals in sediments. *Geochim. Cosmochim. Acta* 63, 1735–1750. doi: 10.1016/S0016-7037(99)00126-X

Morse, J. W., and Luther, G. W. (1999). Chemical influences on trace metal-sulfide interactions in anoxic sediments. *Geochim. Cosmochim. Acta* 63, 3373–3378. doi: 10.1016/S0016-7037(99)00258-6

Murray, J. W., Grundmanis, V., and Smethie, W. M. (1978). Interstitial water chemistry in the sediments of Saanich Inlet. *Geochim. Cosmochim. Acta* 42, 1011–1026. doi: 10.1016/0016-7037(78)90290-9

Naehr, T. H., Eichhubl, P., Orphan, V. J., Hovland, M., Paull, C. K., Ussler, W. III, et al. (2007). Authigenic carbonate formation at hydrocarbon seeps in continental margin sediments: a comparative study. *Deep. Sea. Res. Part II.* 54, 1268–1291. doi: 10.1016/j.dsr2.2007.04.010

Naehr, T. H., Rodriguez, N., Bohrmann, G., Paull, C., and Botz, R. (2000). Methane-derived authigenic carbonates associated with gas hydrate decomposition and fluid venting above the Blake Ridge Diapir. *Proc. ODP. Sci. Results.* 164, 285–300. doi: 10.2973/odp.proc.sr.164.228.2000

Nealson, K. H., and Saffarini, D. (1994). Iron and manganese in anaerobic respiration: environmental significance, physiology, and regulation. *Annu. Rev. Microbiol.* 48, 311–343. doi: 10.1146/annurev.micro.48.1.311

Niewöhner, C., Hensen, C., Kasten, S., Zabel, M., and Schulz, H. D. (1998). Deep sulfate reduction completely mediated by anaerobic methane oxidation in sediments of the upwelling area off Namibia. *Geochim. Cosmochim. Acta* 62, 455–464. doi: 10.1016/S0016-7037(98)00055-6

Nöthen, K., and Kasten, S. (2011). Reconstructing changes in seep activity by means of pore water and solid phase Sr/Ca and Mg/Ca ratios in pockmark sediments of the northern Congo Fan. *Mar. Geol.* 287, 1–13. doi: 10.1016/j.margeo.2011.06.008

Pälike, C., Delaney, M. L., and Zachos, J. C. (2014). Deep-sea redox across the Paleocene-Eocene Thermal Maximum. *Geochem. Geophys. Geosyst.* 15, 1038–1053. doi: 10.1002/2013GC005074

Paull, C. K., Ussler, W., Lorenson, T., Winters, W., and Dougherty, J. (2005). Geochemical constraints on the distribution of gas hydrates in the Gulf of Mexico. *Geo-Mar. Lett.* 25, 273–280. doi: 10.1007/s00367-005-0001-3

Peckmann, J., Reimer, A., Luth, U., Luth, C., Hansen, B. T., Heinicke, C., et al. (2001). Methane-derived carbonates and authigenic pyrite from the northwestern black sea. *Mar. Geol.* 177, 129–150. doi: 10.1016/S0025-3227(01)00128-1

Peckmann, J., and Thiel, V. (2004). Carbon cycling at ancient methane-seeps. *Chem. Geol.* 205, 443–467. doi: 10.1016/j.chemgeo.2003.12.025

Peckmann, J., Thiel, V., Michaelis, W., Clari, P., Gaillard, C., Martire, L., et al. (1999). Cold seep deposits of Beauvoisin (Oxfordian; southeastern France) and Marmorito (Miocene; northern Italy): Microbially induced authigenic carbonates. *Int. J. Earth Sci.* 88, 60–75. doi: 10.1007/s005310050246

Pehlivanli, B. Y., Koç, Ç., Sari, A., and Engin, H. (2014). Factors controlling low uranium and thorium concentrations in the Çayirhan Bituminous Shales (ÇBS) in the Beypazari (Ankara) area, Turkey. *Acta Geol. Sin. (Engl. Ed.)* 88, 248–259. doi: 10.1111/1755-6724.12195

Peketi, A., Mazumdar, A., Joshi, R. K., Patil, D. J., Srinivas, P. L., and Dayal, A. M. (2012). Tracing the paleo sulfate-methane transition zones and H_2S seepage events in marine sediments: An application of C-S-Mo systematics. *Geochem. Geophys. Geosyst.* 13. doi: 10.1029/2012GC004288

Pierre, C., Bayon, G., Blanc-Valleron, M.-M., Mascle, J., and Dupré, S. (2014). Authigenic carbonates related to active seepage of methane-rich hot brines at the Cheops Mud Volcano, Menes Caldera (Nile Deep-Sea Fan, eastern Mediterranean Sea). *Geo-Mar. Lett.* 34, 253–267. doi: 10.1007/s00367-014-0362-6

Piper, D. Z. (1974). Rare earth elements in the sedimentary cycle: A summary. *Chem. Geol.* 14, 285–304. doi: 10.1016/0009-2541(74)90066-7

Poulton, S. W., and Canfield, D. E. (2011). Ferruginous conditions: A dominant feature of the ocean through Earth's history. *Elements* 7, 107–112. doi: 10.2113/gselements.7.2.107

Pourret, O., Davranche, M., Gruau, G., and Dia, A. (2008). New insights into cerium anomalies in organic-rich alkaline waters. *Chem. Geol.* 251, 120–127. doi: 10.1016/j.chemgeo.2008.03.002

Raghoebarsing, A. A., Pol, A., Van De Pas-Schoonen, K. T., Smolders, A. J. P., Ettwig, K. F., Rijpstra, W. I. C., et al. (2006). A microbial consortium couples anaerobic methane oxidation to denitrification. *Nature* 440, 918–921. doi: 10.1038/nature04617

Reeburgh, W. S. (2007). Oceanic methane biogeochemistry. *Chem. Rev.* 107, 486–513. doi: 10.1021/cr050362v

Riedinger, N., Formolo, M. J., Lyons, T. W., Henkel, S., Beck, A., and Kasten, S. (2014). An inorganic geochemical argument for coupled anaerobic oxidation of methane and iron reduction in marine sediments. *Geobiology* 12, 172–181. doi: 10.1111/gbi.12077

Ritger, S., Carson, B., and Suess, E. (1987). Methane-derived authigenic carbonates formed by subduction-induced pore-water expulsion along the Oregon/Washington margin. *Geol. Soc Am. Bull.* 98, 147. doi: 10.1130/0016-7606(1987)982.0.CO;2

Roberts, A. P. (2015). Magnetic mineral diagenesis. *Earth Sci. Rev.* 151, 1–47. doi: 10.1016/j.earscirev.2015.09.010

Rongemaille, E., Bayon, G., Pierre, C., Bollinger, C., Chu, N. C., Fouquet, Y., et al. (2011). Rare earth elements in cold seep carbonates from the Niger Delta. *Chem. Geol.* 286, 196–206. doi: 10.1016/j.chemgeo.2011.05.001

Rooze, J., Egger, M., Tsandev, I., and Slomp, C. P. (2016). Iron-dependent anaerobic oxidation of methane in coastal surface sediments: Potential controls and impact. *Limnol. Oceanogr.* 61, S267–S282. doi: 10.1002/lno.10275

Russell, A. D., and Morford, J. L. (2001). The behavior of redox-sensitive metals across a laminated–massive–laminated transition in Saanich Inlet, British Columbia. *Mar. Geol.* 174, 341–354. doi: 10.1016/S0025-3227(00)00159-6

Sassen, R., Roberts, H. H., Carney, R., Milkov, A. V., DeFreitas, D. A., Lanoil, B., et al. (2004). Free hydrocarbon gas, gas hydrate, and authigenic minerals in chemosynthetic communities of the northern Gulf of Mexico continental slope: relation to microbial processes. *Chem. Geol.* 205, 195–217. doi: 10.1016/j.chemgeo.2003.12.032

Savard, M. M., Beauchamp, B., and Veizer, J. (1996). Significance of aragonite cements around Cretaceous marine methane seeps. *J. Sediment. Res.* 66, 430–438. doi: 10.1306/D4268365-2B26-11D7-8648000102C1865D

Scherer, P., Lippert, H., and Wolff, G. (1983). Composition of the major elements and trace elements of 10 methanogenic bacteria determined by inductively coupled plasma emission spectrometry. *Biol. Trace Elem. Res.* 5, 149–163. doi: 10.1007/BF02916619

Scott, C., and Lyons, T. W. (2012). Contrasting molybdenum cycling and isotopic properties in euxinic versus non-euxinic sediments and sedimentary rocks: Refining the paleoproxies. *Chem. Geol.* 324–325, 19–27. doi: 10.1016/j.chemgeo.2012.05.012

Shields, G., and Stille, P. (2001). Diagenetic constraints on the use of cerium anomalies as palaeoseawater redox proxies: An isotopic and REE study of Cambrian phosphorites. *Chem. Geol.* 175, 29–48. doi: 10.1016/S0009-2541(00)00362-4

Shields, G. A., and Webb, G. E. (2004). Has the REE composition of seawater changed over geological time? *Chem. Geol.* 204, 103–107. doi: 10.1016/j.chemgeo.2003.09.010

Slomp, C. P., Mort, H. P., Jilbert, T., Reed, D. C., Gustafsson, B. G., and Wolthers, M. (2013). Coupled dynamics of iron and phosphorus in sediments of an oligotrophic coastal basin and the impact of anaerobic oxidation of methane. *PloS One* 8, e62386. doi: 10.1371/journal.pone.006238

Smrzka, D., Feng, D., Himmler, T., Zwicker, J., Hu, Y., Monien, P., et al. (2020). Trace elements in methane-seep carbonates: Potentials, limitations, and perspectives. *Earth Sci. Rev.* 208, 103263. doi: 10.1016/j.earscirev.2020.103263

Smrzka, D., Zwicker, J., Bach, W., Feng, D., Himmler, T., Chen, D., et al. (2019). The behavior of trace elements in seawater, sedimentary pore water, and their incorporation into carbonate minerals: A review. *Facies* 65, 41. doi: 10.1007/s10347-019-0581-4

Snyder, G. T., Hiruta, A., Matsumoto, R., Dickens, G. R., Tomaru, H., Takeuchi, R., et al. (2007). Pore water profiles and authigenic mineralization in shallow marine sediments above the methane-charged system on Umitaka Spur, Japan Sea. *Deep. Sea. Res. Part II.* 54, 1216–1239. doi: 10.1016/j.dsr2.2007.04.001

Su, G., Zopfi, J., Yao, H., Steinle, L., Niemann, H., and Lehmann, M. F. (2020). Manganese/iron-supported sulfate-dependent anaerobic oxidation of methane by archaea in lake sediments. *Limnol. Oceanogr.* 65, 863–875. doi: 10.1002/lno.11354

Sun, Z., Wei, H., Zhang, X., Shang, L., Yin, X., Sun, Y., et al. (2015). A unique Fe-rich carbonate chimney associated with cold seeps in the northern Okinawa Trough, East China Sea. *Deep. Sea. Res. Part I.* 95, 37–53. doi: 10.1016/j.dsr.2014.10.005

Sun, T., Wu, D., Yang, F., Liu, L., Chen, X., and Ye, Y. (2019). Sedimentary geochemical proxies for methane seepage at site C14 in the Qiongdongnan Basin in the northern South China Sea. *Acta Oceanol. Sin.* 38, 84–95. doi: 10.1007/s13131-019-1460-6

Tanaka, K., Akagawa, F., Yamamoto, K., Tani, Y., Kawabe, I., and Kawai, T. (2007). Rare earth element geochemistry of Lake Baikal sediment: Its implication for geochemical response to climate change during the last glacial/interglacial transition. *Quat. Sci. Rev.* 26, 1362–1368. doi: 10.1016/j.quascirev.2007.02.004

Taylor, S. R., and McClennan, S. M. (1985). *The continental crust: Its composition and evolution: an examination of the geochemical record preserved in sedimentary rocks* (Oxford: Blackwell Scientific).

Tesoriero, A. J., and Pankow, J. F. (1996). Solid solution partitioning of Sr^{2+}, Ba^{2+}, and Cd^{2+} to calcite. *Geochim. Cosmochim. Acta* 60, 1053–1063. doi: 10.1016/0016-7037(95)00449-1

Thiel, V., Peckmann, J., Richnow, H. H., Luth, U., Reitner, J., and Michaelis, W. (2001). Molecular signals for anaerobic methane oxidation in Black Sea seep carbonates and a microbial mat. *Mar. Chem.* 73, 97–112. doi: 10.1016/S0304-4203(00)00099-2

Torres, M. E., Bohrmann, G., Dubé, T. E., and Poole, F. G. (2003). Formation of modern and Paleozoic stratiform barite at cold methane seeps on continental margins. *Geology* 31, 897. doi: 10.1130/G19652.1

Torres, M. E., Bohrmann, G., and Suess, E. (1996). Authigenic barites and fluxes of barium associated with fluid seeps in the Peru subduction zone. *Earth Planet. Sci. Lett.* 144, 469–481. doi: 10.1016/S0012-821X(96)00163-X

Torres, M. E., McManus, J., and Huh, C.-A. (2002). Fluid seepage along the San Clemente Fault Scarp: Basin-wide impact on barium cycling. *Earth Planet. Sci. Lett.* 203, 181–194. doi: 10.1016/S0012-821X(02)00800-2

Tribovillard, N., Algeo, T. J., Baudin, F., and Riboulleau, A. (2012). Analysis of marine environmental conditions based on molybdenum–uranium covariation—applications to Mesozoic paleoceanography. *Chem. Geol.* 324–325, 46–58. doi: 10.1016/j.chemgeo.2011.09.009

Tribovillard, N., Algeo, T. J., Lyons, T., and Riboulleau, A. (2006). Trace metals as paleoredox and paleoproductivity proxies: An update. *Chem. Geol.* 232, 12–32. doi: 10.1016/j.chemgeo.2006.02.012

Tribovillard, N., Du Châtelet, E. A., Gay, A., Barbecot, F., Sansjofre, P., and Potdevin, J.-L. (2013). Geochemistry of cold seepage-impacted sediments: Per-ascensum or per-descensum trace metal enrichment? *Chem. Geol.* 340, 1–12. doi: 10.1016/j.chemgeo.2012.12.012

Tyson, R. V., and Pearson, T. H. (1991). Modern and ancient continental shelf anoxia: an overview. *Geol. Soc Lond. Spec. Publ.* 58, 1–24. doi: 10.1144/GSL.SP.1991.058.01.01

Ussler, W. III, and Paull, C. K. (2008). Rates of anaerobic oxidation of methane and authigenic carbonate mineralization in methane-rich deep-sea sediments inferred from models and geochemical profiles. *Earth Planet. Sci. Lett.* 266, 271–287. doi: 10.1016/j.epsl.2007.10.056

Vanneste, H., James, R. H., Kelly-Gerreyn, B. A., and Mills, R. A. (2013). Authigenic barite records of methane seepage at the Carlos Ribeiro Mud Volcano (Gulf of Cadiz). *Chem. Geol.* 354, 42–54. doi: 10.1016/j.chemgeo.2013.06.010

Wallenius, A. J., Dalcin Martins, P., Slomp, C. P., and Jetten, M. S. M. (2021). Anthropogenic and environmental constraints on the microbial methane cycle in coastal sediments. *Front. Microbiol.* 12. doi: 10.3389/fmicb.2021.631621

Wang, X., Bayon, G., Kim, J.-H., Lee, D.-H., Kim, D., Guéguen, B., et al. (2019). Trace element systematics in cold seep carbonates and associated lipid compounds. *Chem. Geol.* 528, 119277. doi: 10.1016/j.chemgeo.2019.119277

Wang, S., Magalhães, V. H., Pinheiro, L. M., Liu, J., and Yan, W. (2015). Tracing the composition, fluid source and formation conditions of the methane-derived authigenic carbonates in the Gulf of Cadiz with rare earth elements and stable isotopes. *Mar. Pet. Geol.* 68, 192–205. doi: 10.1016/j.marpetgeo.2015.08.022

Wang, Q., Tong, H., Huang, C.-Y., and Chen, D. (2018). Tracing fluid sources and formation conditions of Miocene hydrocarbon-seep carbonates in the central western foothills, central Taiwan. *J. Asian Earth Sci.* 168, 186–196. doi: 10.1016/j.jseaes.2017.11.015

Wang, S., Yan, W., Chen, Z., Zhang, N., and Chen, H. (2014). Rare earth elements in cold seep carbonates from the southwestern Dongsha area, northern South China Sea. *Mar. Pet. Geol.* 57, 482–493. doi: 10.1016/j.marpetgeo.2014.06.017

Waseda, A. (1998). Organic carbon content, bacterial methanogenesis, and accumulation processes of gas hydrates in marine sediments. *Geochem. J.* 32, 143–157. doi: 10.2343/geochemj.32.143

Wilde, P., Quinby-Hunt, M. S., and Erdtmann, B.-D. (1996). The whole-rock cerium anomaly: A potential indicator of eustatic sea-level changes in shales of the anoxic facies. *Sediment. Geol.* 101, 43–53. doi: 10.1016/0037-0738(95)00020-8

Wilfert, P., Krause, S., Liebetrau, V., Schönfeld, J., Haeckel, M., Linke, P., et al. (2015). Response of anaerobic methanotrophs and benthic foraminifera to variable methane supply at a cold seep in the North Sea. *Mar. Pet. Geol.* 68, 731–742. doi: 10.1016/j.marpetgeo.2015.07.012

Wright, J., Schrader, H., and Holser, W. T. (1987). Paleoredox variations in ancient oceans recorded by rare earth elements in fossil apatite. *Geochim. Cosmochim. Acta* 51, 631–644. doi: 10.1016/0016-7037(87)90075-5

Wu, D., Xie, R., Liu, J., Yang, F., Sun, T., Liu, L., et al. (2020). Zone of metal-driven anaerobic oxidation of methane is an important sink for phosphorus in the Taixinan Basin, South China Sea. *Mar. Geol.* 427, 106268. doi: 10.1016/j.margeo.2020.106268

Wu, D., Yang, F., Huang, X., Pan, M., Sun, T., Liu, L., et al. (2017). Rare earth elemental geochemistry of the sediments in cold-seep area in Dongsha area of South China Sea. *Mar. Geol. Quat. Geol.* 37, 59–69. doi: 10.16562/j.cnki.0256-1492.2017.05.006

Xiao, X., Luo, M., Zhang, C., Zhang, T., Yin, X., Wu, X., et al. (2023). Metal-driven anaerobic oxidation of methane as an important methane sink in methanic cold seep sediments. *Microbiol. Spectr.* 11, e05337–e05322. doi: 10.1128/spectrum.05337-22

Xue, Y., Lu, H., Li, Y., Yang, H., Tang, Y., and Lu, Y. (2025). Anaerobic oxidation of methane by manganese oxides in marine sediments: A review. *Front. Mar. Sci.* 12. doi: 10.3389/fmars.2025.1609892

Yang, K. H., Chu, F. Y., Ye, L. M., Zhang, W. Y., Xu, D., Zhu, J. H., et al. (2014). Implication of methane seeps from sedimentary geochemical proxies (Sr/Ca and Mg/Ca) in the northern South China Sea. *J. Jilin. Univ. (Earth. Sci. Ed.)* 44, 469–479. doi: 10.13278/j.cnki.jjuese.201402106

Yang, S. Y., and Li, C. X. (1999). Progress on the study of sediment source tracing using REE. *Adv. Earth Sci.* 14, 164–167. doi: 10.11867/j.issn.1001-8166.1999.02.0164

Yang, H., Lu, H., and Ruffine, L. (2018). Geochemical characteristics of iron in sediments from the Sea of Marmara. *Deep. Sea. Res. Part II.* 153, 121–130. doi: 10.1016/j.dsr2.2018.01.010

Yang, H., Zhang, P., Lu, H., Shi, M., Li, J., Lu, Y., et al. (2023). Magnetic properties of gas hydrate-bearing sediments and their association with iron geochemistry in the Sea of Marmara, Turkey. *Chem. Geol.* 620, 121339. doi: 10.1016/j.chemgeo.2023.121339

Yao, H., Niemann, H., and Panieri, G. (2020). Multi-proxy approach to unravel methane emission history of an Arctic cold seep. *Quat. Sci. Rev.* 244, 106490. doi: 10.1016/j.quascirev.2020.106490

Yarincik, K. M., Murray, R. W., Lyons, T. W., Peterson, L. C., and Haug, G. H. (2000). Oxygenation history of bottom waters in the Cariaco Basin, Venezuela, over the past 578,000 years: Results from redox-sensitive metals (Mo, V, Mn, and Fe). *Paleoceanography* 15, 593–604. doi: 10.1029/1999PA000401

Zhu, B., Ge, L., Yang, T., Jiang, S. Y., and Lv, X. (2019). Stable isotopes and rare earth element compositions of ancient cold seep carbonates from Enza River, northern Apennines (Italy): Implications for fluids sources and carbonate chimney growth. *Mar. Pet. Geol.* 110, 563–576. doi: 10.1016/j.marpetgeo.2019.06.033

Glossary

ANME	Anaerobic Methanotrophic Archaea
AOM	Anaerobic Oxidation of Methane
DIC	Dissolved Inorganic Carbon
EF	Enrichment Factor
Fe-AOM	Iron-Dependent Anaerobic Oxidation of Methane
HREE	Heavy Rare Earth Elements
LREE	Light Rare Earth Elements
MDAC	Methane-Derived Authigenic Carbonate
Mn-AOM	Manganese-Dependent Anaerobic Oxidation of Methane
MnR-AOM	Manganese Reduction-Coupled Anaerobic Oxidation of Methane
MnR-S-AOM	Manganese Reduction-Coupled Sulfur-Dependent Anaerobic Oxidation of Methane
MO	Methane Oxidation
MOB	Aerobic Methane-Oxidizing Bacteria
MOG	Methanogenesis
MREE	Middle Rare Earth Elements
MSR	Microbial Sulfate Reduction
OSR	Organoclastic Sulfate Reduction
PAAS	Post Archean Australian Shale
REE	Rare Earth Elements
SD-AOM	Sulfate-Driven Anaerobic Oxidation of Methane
SMI	Sulfate-Methane Transition Interface
SMTZ	Sulfate-Methane Transition Zone
SR	Sulfate Reduction
SRB	Sulfate-Reducing Bacteria
SWI	Sea-Water Interface
TGHSZ	The Top of Gas Hydrate Stability Zone
TIC	Total Inorganic Carbon
TOC	Total Organic Carbon
TS	Total Sulfur